

# **JGR** Solid Earth



#### RESEARCH ARTICLE

10.1029/2023JB027938

#### **Key Points:**

- Estimates of water storage made at fine spatial scales are highly sensitive to the Earth model used to invert geodetic measurements
- Sensitivities to Earth structure produce uncertainties in estimates of water storage that scale with the total weight of the water load
- Predictions of uplift produced by melting of the Earth's ice sheets over the past two decades can differ by over 20 mm between Earth models

#### **Supporting Information:**

Supporting Information may be found in the online version of this article.

#### Correspondence to:

M. J. Swarr, matthew.swarr@umontana.edu

#### Citation:

Swarr, M. J., Martens, H. R., & Fu, Y. (2024). Sensitivity of GNSS-derived estimates of terrestrial water storage to assumed Earth structure. *Journal of Geophysical Research: Solid Earth, 129*, e2023JB027938. https://doi.org/10.1029/2023JB027938

Received 27 SEP 2023 Accepted 24 FEB 2024

### **Author Contributions:**

Conceptualization: Matthew J. Swarr, Hilary R. Martens, Yuning Fu Data curation: Matthew J. Swarr Formal analysis: Matthew J. Swarr, Hilary R. Martens

**Funding acquisition:** Hilary R. Martens, Yuning Fu

Methodology: Matthew J. Swarr, Hilary R. Martens

Project administration: Hilary R. Martens, Yuning Fu Software: Matthew J. Swarr, Hilary R. Martens

**Supervision:** Hilary R. Martens **Visualization:** Matthew J. Swarr

#### © 2024. The Authors.

This is an open access article under the terms of the Creative Commons Attribution-NonCommercial-NoDerivs License, which permits use and distribution in any medium, provided the original work is properly cited, the use is non-commercial and no modifications or adaptations are made.

## Sensitivity of GNSS-Derived Estimates of Terrestrial Water Storage to Assumed Earth Structure

Matthew J. Swarr<sup>1</sup>, Hilary R. Martens<sup>1</sup>, and Yuning Fu<sup>2</sup>

<sup>1</sup>Department of Geosciences, University of Montana, Missoula, MT, USA, <sup>2</sup>School of Earth, Environment and Society, Bowling Green State University, Bowling Green, OH, USA

**Abstract** Geodetic methods can monitor changes in terrestrial water storage (TWS) across large regions in near real-time. Here, we investigate the effect of assumed Earth structure on TWS estimates derived from Global Navigation Satellite System (GNSS) displacement time series. Through a series of synthetic tests, we systematically explore how the spatial wavelength of water load affects the error of TWS estimates. Large loads (e.g., >1,000 km) are well recovered regardless of the assumed Earth model. For small loads (e.g., <10 km), however, errors can exceed 75% when an incorrect model for the Earth is chosen. As a case study, we consider the sensitivity of seasonal TWS estimates within mountainous watersheds of the western U.S., finding estimates that differ by over 13% for a collection of common global and regional structural models. Errors in the recovered water load generally scale with the total weight of the load; thus, long-term changes in storage can produce significant uplift (subsidence), enhancing errors. We demonstrate that regions experiencing systematic and large-scale variations in water storage, such as the Greenland ice sheet, exhibit significant differences in predicted displacement (over 20 mm) depending on the choice of Earth model. Since the discrepancies exceed GNSS observational precision, an appropriate Earth model must be adopted when inverting GNSS observations for mass changes in these regions. Furthermore, regions with large-scale mass changes that can be quantified using independent data (e.g., altimetry, gravity) present opportunities to use geodetic observations to refine structural properties of seismologically derived models for the Earth's interior structure.

Plain Language Summary In many regions of the Earth, water resources used for agriculture, domestic, and industrial purposes rely on stream flow and groundwater sourced from the melting of winter snowpack in adjacent mountains. Modern shifts in climate have resulted in increasingly variable precipitation patterns and temperatures during winter months. Coupled with a rising global population, there has been a growing need for accurate estimates of freshwater stored above and beneath the land surface. A relatively new interdisciplinary approach called hydrogeodesy allows for freshwater resources to be monitored by using satellite- and ground-based sensors to accurately measure changes in the shape and gravitational field of the Earth produced by the redistribution of water between hydrologic reservoirs. As this approach becomes increasingly utilized to inform decision-makers, however, we require a deeper understanding of the assumptions and uncertainties of the models used to translate between geodetic measurements and estimates of water storage. Here, we consider the impact of assumptions about the Earth's interior structure on the error of geodetic water storage estimates. We present a set of case studies that display the varied influence of assumed Earth structure on water storage estimates depending on the spatial scale and amplitude of water storage variations.

#### 1. Introduction

Accurate estimates of terrestrial water storage (TWS), defined as the sum of all storage within surface and subsurface reservoirs, are vital in the assessment and effective long-term management of water resources. In addition, accurate assessment of TWS aids in our understanding of the Earth's water cycle and interactions between individual hydrological reservoirs, such as snowpack and groundwater (e.g., Enzminger et al., 2019; Lettenmaier & Famiglietti, 2006). Recent developments in space geodesy, such as the Global Navigation Satellite Systems (GNSS), have become increasingly important in the study of freshwater resources as accurate measurement of subtle changes in the shape and gravitational field of the Earth produced by the redistribution of mass within surface and subsurface hydrologic reservoirs allow for spatially distributed estimates of TWS to be made at local and regional scales (e.g., Argus et al., 2014; Argus et al., 2022; Milliner et al., 2018; Wahr et al., 2004) complementing other data sets currently used in the assessment and management of water resources.

SWARR ET AL. 1 of 21



## Journal of Geophysical Research: Solid Earth

10.1029/2023JB027938

Writing – original draft: Matthew J. Swarr Writing – review & editing: Matthew J. Swarr, Hilary R. Martens, Yuning Fu Most geodetic investigations of TWS, however, have not considered the impact of the choice of Earth structure model on water storage estimates, which may lead to inaccuracies in estimated TWS and misinformed decision-making by water managers and policymakers. The deformation response of the Earth due to variations in TWS is controlled by the spatiotemporal characteristics of the hydrologic surface mass as well as the material properties of the Earth's interior. To translate between observations of surface displacement and changes in storage within hydrologic reservoirs, prior knowledge of the Earth's elastic and density structure is required to accurately predict displacement of the Earth's surface to an applied load (e.g., Farrell, 1972; Martens et al., 2019). A majority of studies using GNSS observations to estimate TWS have used globally averaged estimates of Earth structure, such as PREM (Dziewonski & Anderson, 1981) or Gutenberg-Bullen (Alterman et al., 1961), to map between observations of surface displacement and estimates of TWS (e.g., Argus et al., 2014, 2017; Borsa et al., 2014; Enzminger et al., 2018).

Recent studies suggest that displacements produced by changes in surface mass can be highly sensitive to the local material properties and structural features of the crust and upper mantle, especially for surface loading occurring at relatively fine spatial scales (e.g., < 2,500 km²) (e.g., Dill et al., 2015; Martens, Simons, et al., 2016). For example, Martens, Rivera, et al. (2016) computed sensitivity kernels for the load Love number (LLNs) and load Green's function (LGFs), which describe the deformation response of the Earth to an applied unit point load, by systematically perturbing the elastic and density structure of PREM through the crust and upper mantle, finding the LGFs to be predominately sensitive to variations in elastic material properties in the upper 500 km of the Earth. Further, Dill et al. (2015) quantified the effect of sensitivities to local crustal structure on the deformation response to surface loading using grids of local LGFs, finding magnitudes of differences up to 25% for vertical displacement and 91% for horizontal displacement. Such sensitivities offer the possibility of tomographic studies to refine seismologically derived Earth models' structural properties when the loading source is reasonably constrained, such as the Earth's ocean tides (e.g., Ito & Simons, 2011). In the interest of using GNSS observations to better manage water resources across various spatial scales (e.g., continental-scale vs. watershed-scale), assumptions about the Earth's interior structure may significantly bias TWS estimates depending on the spatial scale of interest due to sensitivities to the shallow material properties of the Earth, which can differ significantly across regions.

The uncertainty of TWS estimates associated with choice of Earth structure has only recently begun to be explored (e.g., Argus et al., 2017; Dill et al., 2015). For example, Wang et al. (2015) estimated the effect of assumed Earth structure on estimates of TWS derived from synthetic displacement and gravity observations for the Tibetan Plateau. Utilizing a one-dimensional Earth model that reflected the regional crustal structure of the Tibetan Plateau, they produced forward modeled surface displacements from an input hydrologic load model. Following this, an inversion of the synthetic displacements revealed that only 88% of the input load could be recovered when using an a priori Earth model that differed from the one-dimensional local crustal structure of the Tibetan Plateau. However, the study was limited to a single load size that spanned the area of the Tibetan Plateau (~2.5 million km²).

Here, we systematically investigate the sensitivity of surface loading to assumed Earth structure to assess the associated implications in using geodetic measurements to estimate changes in storage within hydrologic reservoirs. We quantify the sensitivity of GNSS-inferred TWS estimates to assumed Earth structure through a series of synthetic tests where displacements produced by surface loads with varying spatial wavelength are inverted while assuming a suite of different reference Earth models. We then present a case study for the western U.S., where we examine nearly two decades of seasonal TWS estimates produced from a variety of global and regional Earth models. Finally, we consider the impact of assumed Earth structure on predicted surface displacement in regions experiencing long-term (i.e., interannual to decadal) changes in storage and identify regions where GNSS-inferred estimates of hydrologic and cryospheric loading may be significantly biased unless an appropriate model for the interior structure of the Earth is adopted. Our use of the term "sensitivity" throughout this work differs from a formal sensitivity analysis, which would measure changes in outputs relative to perturbations in Earth structure parameters (e.g., Martens, Rivera, et al., 2016). Here, "sensitivity" refers to the magnitude of differences in estimates of TWS or predictions of surface displacement when using different Earth models, with larger differences indicating a greater influence of the choice of Earth model on the results.

### 2. Synthetic Tests

To quantify the sensitivity of GNSS-inferred TWS estimates to assumed Earth structure, we carry out a series of synthetic tests which closely reflect the process and underlying logic applied when using real GNSS data to

SWARR ET AL. 2 of 21

estimate changes in TWS. We create a set of synthetic surface displacements for a single spherically symmetric, non-rotating, elastic, and isotropic (SNREI) Earth model, which we take to be the unknown true structure of the Earth. We then invert the synthetic displacements for estimates of TWS while assuming another SNREI Earth model in the design matrix of our inversion. By simulating scenarios where the assumed model for Earth structure differs from the true structure, we can quantify the error in TWS estimates associated with the choice of an incorrect a priori SNREI Earth model used in the inversion. Furthermore, by systematically varying the spatial wavelength of the loads used here, we assess the scale dependencies of the errors. To gain insight into how local crust and upper mantle structure, which can differ significantly from globally averaged estimates of Earth structure, affect estimates of TWS, we consider radially symmetric Earth models based on both globally and regionally relevant structure in our comparisons.

As vertical displacement of the Earth's surface produced by variations in surface loading tends to be higher amplitude than horizontal displacement and less likely to be contaminated by other sources of surface deformation, such as tectonic motion (White et al., 2022), we initially focus our analysis on TWS estimates derived from vertical displacement of the Earth's surface. We note, however, that the inclusion of hydrologically induced horizontal displacements in the inversion (provided that noise and other signal contaminants could be effectively mitigated) would augment the data vector and potentially improve the accuracy and spatial localization of TWS estimates (e.g., Milliner et al., 2018). Therefore, we also consider the impact of including horizontal displacements on estimates of TWS for different Earth models in Supporting Information \$1.

#### 2.1. Earth Models

To provide a broad sample of structural models for the Earth's interior, we consider common reference Earth models: PREM (Dziewonski & Anderson, 1981), AK135f (Kennett et al., 1995; Montagner & Kennett, 1996), STW105 (Kustowski et al., 2008), and 1066A (Gilbert & Dziewonski, 1975), which represent globally averaged estimates of Earth structure (Figure 1). The largest differences between these models are found in the crust and upper mantle; in particular, PREM contains a discontinuity at 220 km depth which the other models do not contain. Additionally, we consider regional Earth models: CR (Chu et al., 2012) and SNA (Grand & Helmberger, 1984), which represent cratonic and stable North American structures that tend to have more rigid elastic structures in the upper mantle compared to the other models considered here. For SNA and CR, beneath approximately 1,000 km depth we assume the material properties of AK135f. Lastly, we consider models derived from LITHO1.0 which reflect local crustal and upper mantle structure on a 1° tessellated global grid (Pasyanos et al., 2014). We consider LITHO1.0 models within the western U.S. as there is a variety of geologic settings within the region (e.g., sedimentary basins, mountain ranges) and later sections of the work presented here are concerned with quantifying the effect of assumed Earth structure on GNSS-inferred TWS estimates within specific mountain provinces of the region.

From LITHO1.0, three local one-dimensional Earth models were constructed to represent the average local crust and upper mantle structure of the San Joaquin, Sacramento, Tulare (SST) River Basin, the Sierra Nevada, and the Cascade Range respectively. For each local model, we consider multiple LITHO1.0 models within the region to produce an estimate of the average local lithospheric structure. The sampling locations in which the local crustal models were derived from LITHO1.0 as well as the local lithosphere thicknesses, below which we assume the material properties of AK135f, are displayed in Table S1 in Supporting Information S1. For models that contain an ocean layer at the surface, we combine the material properties of the ocean layer and uppermost crustal layer to form a single homogeneous layer. The density of the top layer is equal to the weighted mean density of the two original layers, which conserves total mass, and the elastic moduli are equal to those of the original uppermost crustal layer (Guo et al., 2004; Martens & Simons, 2020).

Using LoadDef (Martens et al., 2019), we compute LLNs, LGFs, design matrices, and forward modeled surface displacements. LLNs were computed from spherical harmonic degree n = 0 to n = 1e5 to ensure that the Love Numbers of Earth models with relatively fine sedimentary layers in the uppermost crust converged with the asymptotic approximation of the LLNs. LGFs for each model considered in this manuscript are displayed in Supporting Information S1 of this work (Figure S1). All synthetic surface displacements are computed assuming the Earth model PREM. Thus, we assume PREM represents the true structure of the Earth in the synthetic tests presented here.

SWARR ET AL. 3 of 21

21699356, 2024, 3, Downloaded from https://agupubs. onlinelibrary.wiley.com/doi/10.1029/2023JB027938 by University Of Montana Mansfield Library-Serials, Wiley Online Library on [11/03/2024]. See the Terms and Conditions (https://onlinelibrary.wiley

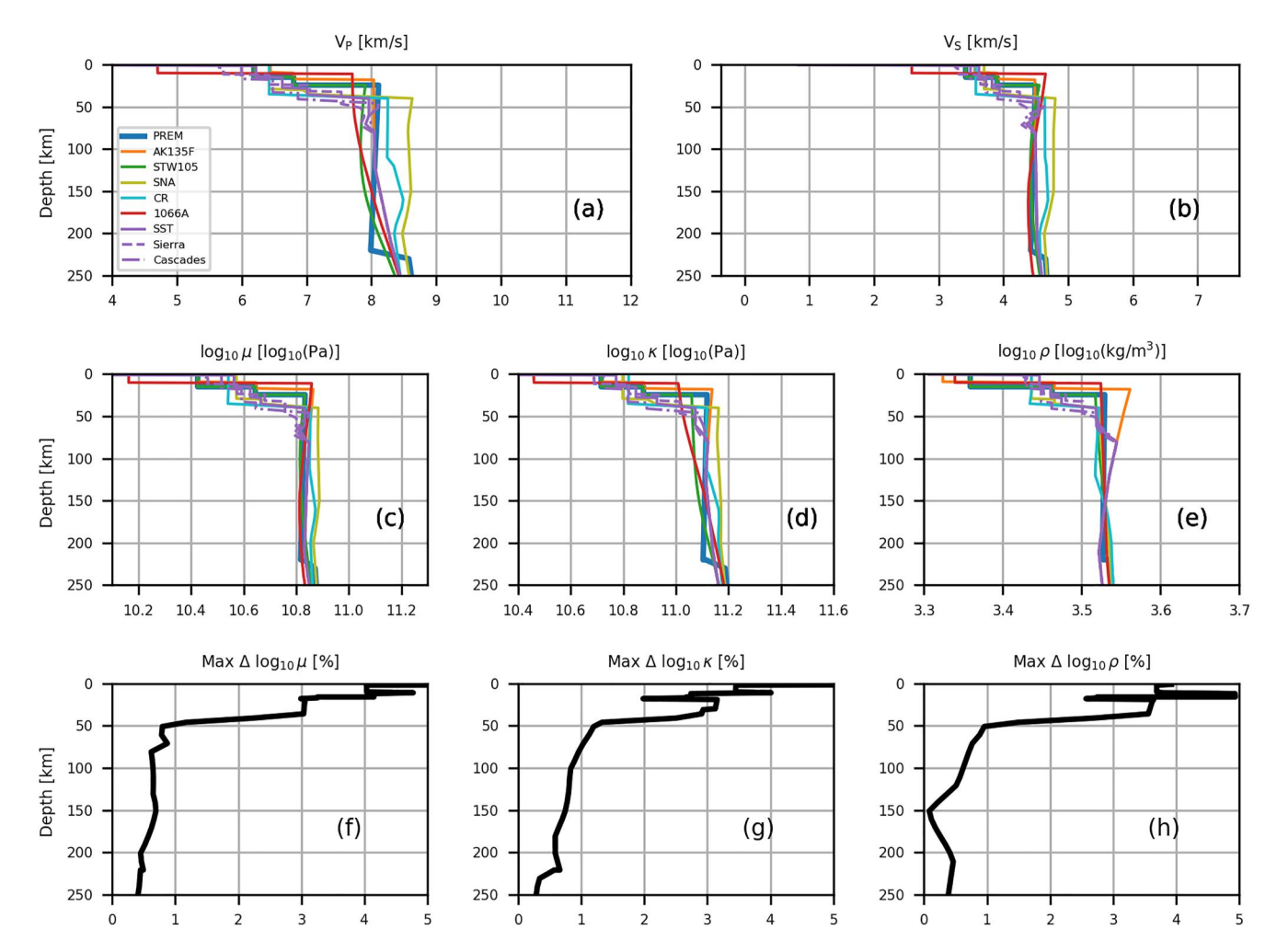


Figure 1. Depth profiles to 250 km depth of one-dimensional Earth models: PREM (blue), AK135f (orange), STW105 (green), SNA (olive), CR (cyan), 1066A (red) as well as models derived from the LITHO1.0 for the San Joaquin, Sacramento, Tulare River Basin (purple) and Sierra Nevada (dashed purple) of California as well as the Cascade Range (dash-dot purple) of Washington, Oregon, and northern California. Panels (a) and (b) show P-wave  $(V_p)$  and S-wave  $(V_q)$  velocity as a function of depth. Panels (c)–(e) show the shear modulus  $(\mu)$ , bulk modulus  $(\kappa)$ , and density  $(\rho)$  profiles in log space. Panels (f)–(h) show the maximum percentage difference between the set of Earth models in log space as a function of depth for the two elastic parameters and density respectively.

#### 2.2. Load Models

We consider Gaussian-shaped surface loads to derive the synthetic surface displacements. The load models represent isotropic bivariate normal distributions with a standard deviation,  $\sigma$ , approximately equal to the Gaussian load's half width at half maximum (HWHM). Each surface load has a maximum height of 1 m of freshwater at its center, which smoothly decays toward zero. For distances greater than four HWHM lengths from the center of the load model, we truncate the load model and consider the load amplitude to be equal to zero. We consider input load models of varying size (HWHMs equivalent to 1, 2.5, ..., 750, 1,000 km) to explore a variety of hydrologically relevant spatial scales.

For each load model, surface displacements were computed for an evenly spaced grid of synthetic GNSS stations, (a/8) km  $\times$  (a/8) km resolution, where a is the HWHM of the respective input load model. Synthetic displacements were computed with respect to the center of mass of the solid Earth, commonly referred to as the CE reference frame (Blewitt, 2003). Additionally, we consider the predicted displacements used in these synthetic examples to be noise-free, which allows for the sensitivity of TWS estimates to Earth structure alone to be isolated. The input load model, distribution of synthetic GNSS stations, and predicted displacements for a 10 km HWHM load are shown in Figure 2.

SWARR ET AL. 4 of 21

2169358, 2024, 3, Downloaded from https://agupubs. onlinelibrary.viley.com/doi/10.1092/0231B027988 by University Of Montana Mansfeld.Library-Serials, Wiley Online Library on [1103/0204]. See the Terms and Conditions (https://onlinelibrary.viley.com/ein/enand-conditions) on Wiley Online Library.

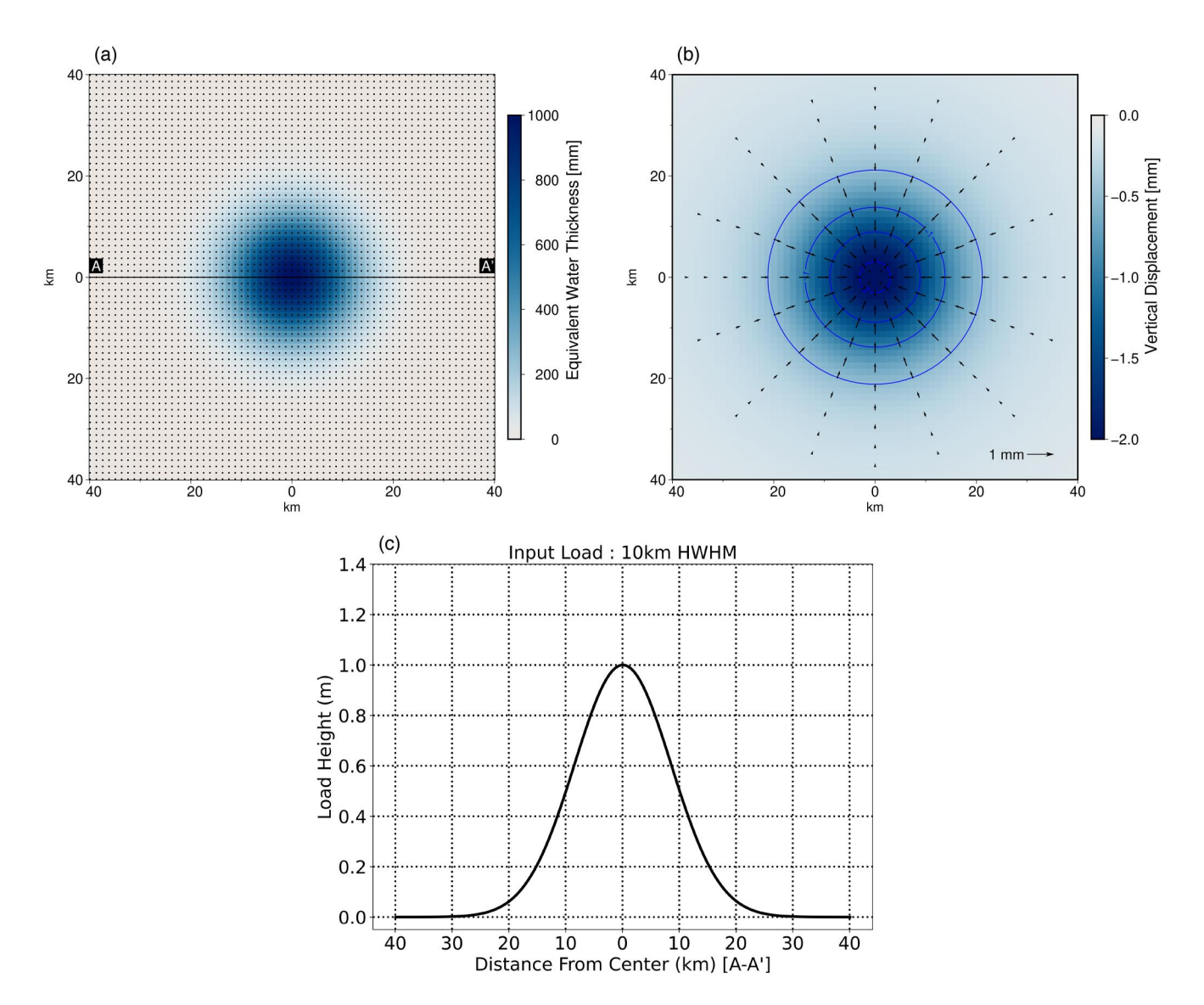


**Figure 2.** (a) 10 km HWHM Gaussian load model used for synthetic loading tests. Black dots represent the locations of synthetic GNSS stations used to produce the synthetic vertical displacements assuming the material properties of PREM as well for estimating surface mass loading utilizing a suite of other one-dimensional Earth models described in Section 2.1. The load amplitude, denoted by the left color bar, represents the height of freshwater distributed evenly within each pixel of the input load model (1.25 km × 1.25 km resolution). Subsequent figures display estimated surface load and error along the profile line (A—A'). (b) Forward modeled vertical and horizontal displacement produced through the convolution of the LGFs of PREM with the load model depicted in (a). Vertical displacement is denoted by the right color bar. Blue contour lines represent 0.5 mm intervals of negative (or downward) vertical displacement. The magnitude and direction of horizontal displacement produced by the load model are depicted as black vectors, with a reference vector located in the lower right corner of panel (b). (c) Input surface load along the profile A-A'.

#### 2.3. Inverse Model

For each load model and synthetic station grid, we perform an inversion of the synthetic displacements to estimate the input surface load. The recovered load height is assumed to be uniform within every grid cell of the inversion grid. We solve for the load within each grid cell by minimizing the damped least squares problem:

$$||(G_i m - d)||_2^2 + \alpha^2 ||(Lm)||_2^2$$
 (1)

where  $G_i$  is the  $[n \times m]$  design matrix containing the predicted elastic response of assumed Earth structure i at each synthetic GNSS station to 1 m of freshwater placed in each grid cell of the model grid, m is the  $[m \times 1]$  vector of unknown quantity of water distributed uniformly within each grid cell, d is the  $[n \times 1]$  vector of synthetic displacements at each station assuming PREM structure (either vertical only or a combination of vertical and

SWARR ET AL. 5 of 21



## Journal of Geophysical Research: Solid Earth

10.1029/2023JB027938

horizontal displacements), L is a 2-D finite difference Laplacian operator used to enforce smoothness between neighboring grid cells, and  $\alpha$  is a regularization parameter, where higher  $\alpha$  values result in smoother variations in estimated surface mass between adjacent grid cells (Aster et al., 2019).

To isolate discrepancies in surface load estimates stemming solely from Earth structure differences between models, we mitigate potential bias from the use of the Laplacian operator and edge effects through two specific measures.

First, to avoid bias introduced by the Laplacian operator, we construct load-model grids of equal resolution to that of the synthetic station grid, where there is one synthetic GNSS station located at the center of each model grid cell. This ensures that the number of observations n is equal to the number of model parameters m being solved for, making the linear system even-determined with a unique solution. As a result, the regularization parameter,  $\alpha$ , of Equation 1 is set equal to zero.

Second, to address unwanted edge effects, we alter the original boundary of our model domain to extend eight half width lengths from the center of each load model. Upon solving Equation 2, we then only consider model grid cells within four half width lengths from the center of the load model for further analysis. Similar to previous studies, we find estimates of surface load to be sensitive to the location of the model domain's boundaries (e.g., Fu et al., 2015). When the edge of the model domain is not extended from its original position, we observe the value of estimated surface load within grid cells along the edge of the domain to be nearly 30% greater than the true value represented by the input load model.

To quantify the sensitivity of GNSS-inferred TWS estimates to assumed Earth structure, we compute the error,  $m_i - m_{true}$ , between the estimated surface load, produced assuming Earth structure i, and the true load model used to produce the synthetic displacements used in Equation 2. We display estimates of surface load derived from the suite of Earth models considered here as well as their error relative to the true load's value along a profile, which crosses the center of each load model (A-A') (Figure 2).

#### 2.4. Effect of Assumed Earth Structure on Estimated Surface Loading

Estimated surface load derived from vertical displacements and error profiles for select load models are displayed in Figure 3. Relative error between estimates of surface load and the *true* load model is largest at relatively fine loading scales (e.g., <10 km HWHM), where the height of the *true* load can be incorrectly estimated by over 75% at the center of the load for select Earth models (Figures 3 and 4). Similarly, we find for loads with relatively small spatial wavelengths, errors in the recovered load can span the entire area of the load model (e.g., Figure 3b). In comparison, as the spatial wavelength of the surface load becomes progressively large, error in recovered load is primarily concentrated within one half width length from the center of the load and is near zero for distances beyond this (e.g., Figure 3h).

As the Earth's response to surface loading occurring at relatively fine spatial scales is predominately controlled by the shallow material properties of the Earth (Martens, Rivera, et al., 2016), discrepancies in estimated surface load reported here reflect differences in the Earth model used to construct the design matrices of our inverse problem, which may contain multiple sedimentary layers in the uppermost crust or a deep cratonic keel, and the globally averaged estimate of Earth structure (PREM) used to produce the data vector. Such discrepancies are most apparent for Earth models that represent regional estimates of structure, such as CR and SNA, or those representing the local crustal structure of specific regions within the western U.S., which differ significantly from the upper crustal structure of PREM (Figure 1). Additional surface load and error profiles for surface loads characterized by other spatial wavelengths considered as a part of this work are provided in Supporting Information S1 (Figures S2–S5).

We therefore find that an incorrect assumption about the material properties of the Earth may yield highly incorrect estimates of surface load when estimating changes in storage within hydrologic reservoirs occurring over short distances and that errors associated with assumed Earth structure diminish as the spatial wavelength of loading becomes increasingly large (Figure 4a). Errors tend to be less than 10% of the *true* load's value when considering surface loads with a HWHM greater than 10 km and become even smaller, less than 2%, as the load HWHM approaches 1,000 km. Such findings are consistent with an increasing sensitivity to Earth structure over broader depth ranges as the size of surface loading increases (Martens, Rivera, et al., 2016), which reduces the sensitivity to highly variable shallow Earth structure (Figure 1). Errors for Earth models that differ from PREM over broad depth

SWARR ET AL. 6 of 21

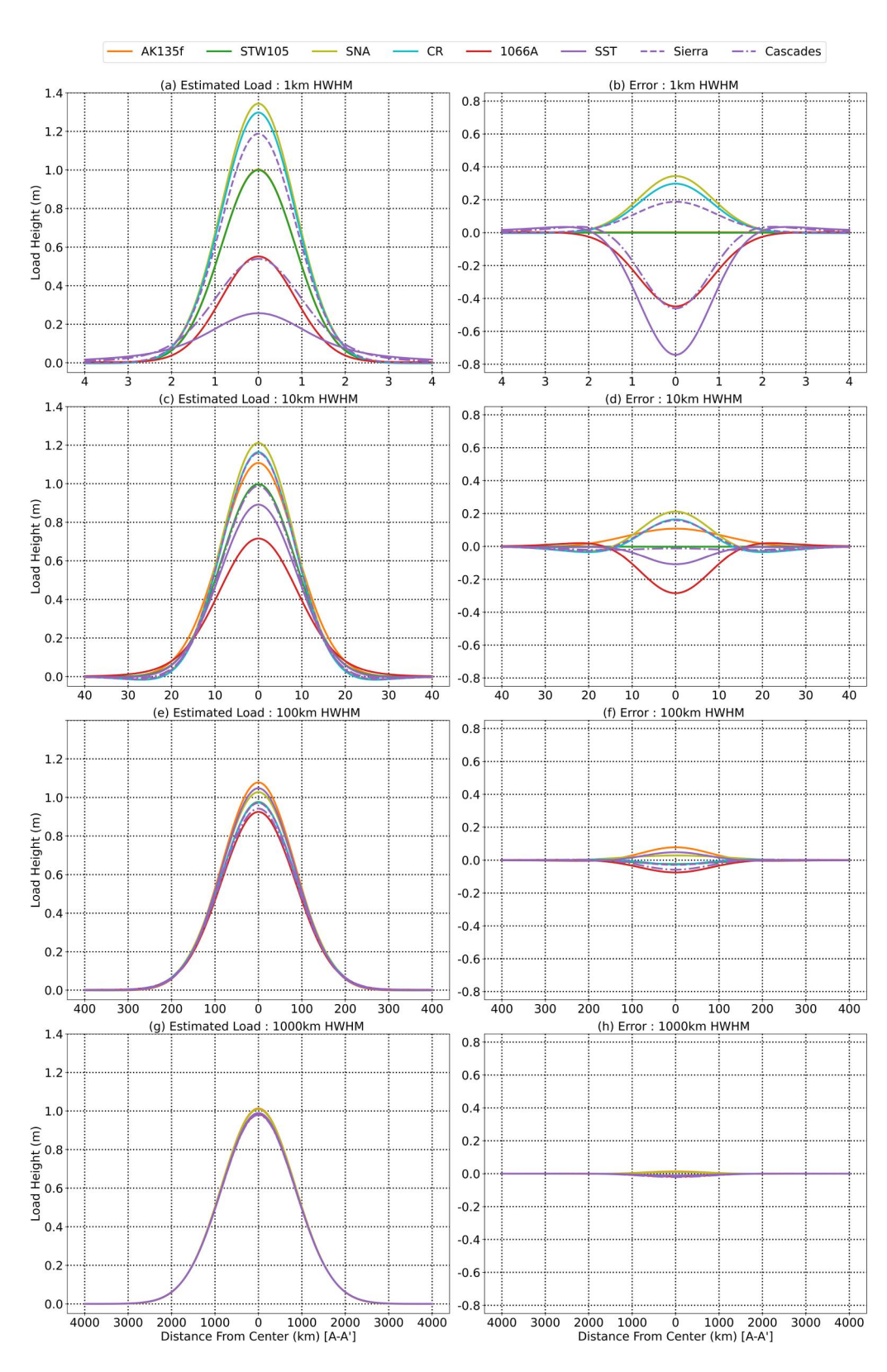


**Figure 3.** Estimated surface load derived from vertical displacements and associated error for inversion estimates assuming the SNREI Earth structures shown in Figure 1 along the profile A-A' in Figure 2 for surface loads corresponding to HWHMs of: (a–b) 1 km, (c–d) 10 km, (e–f) 100 km, and (g–h) 1,000 km.

SWARR ET AL. 7 of 21

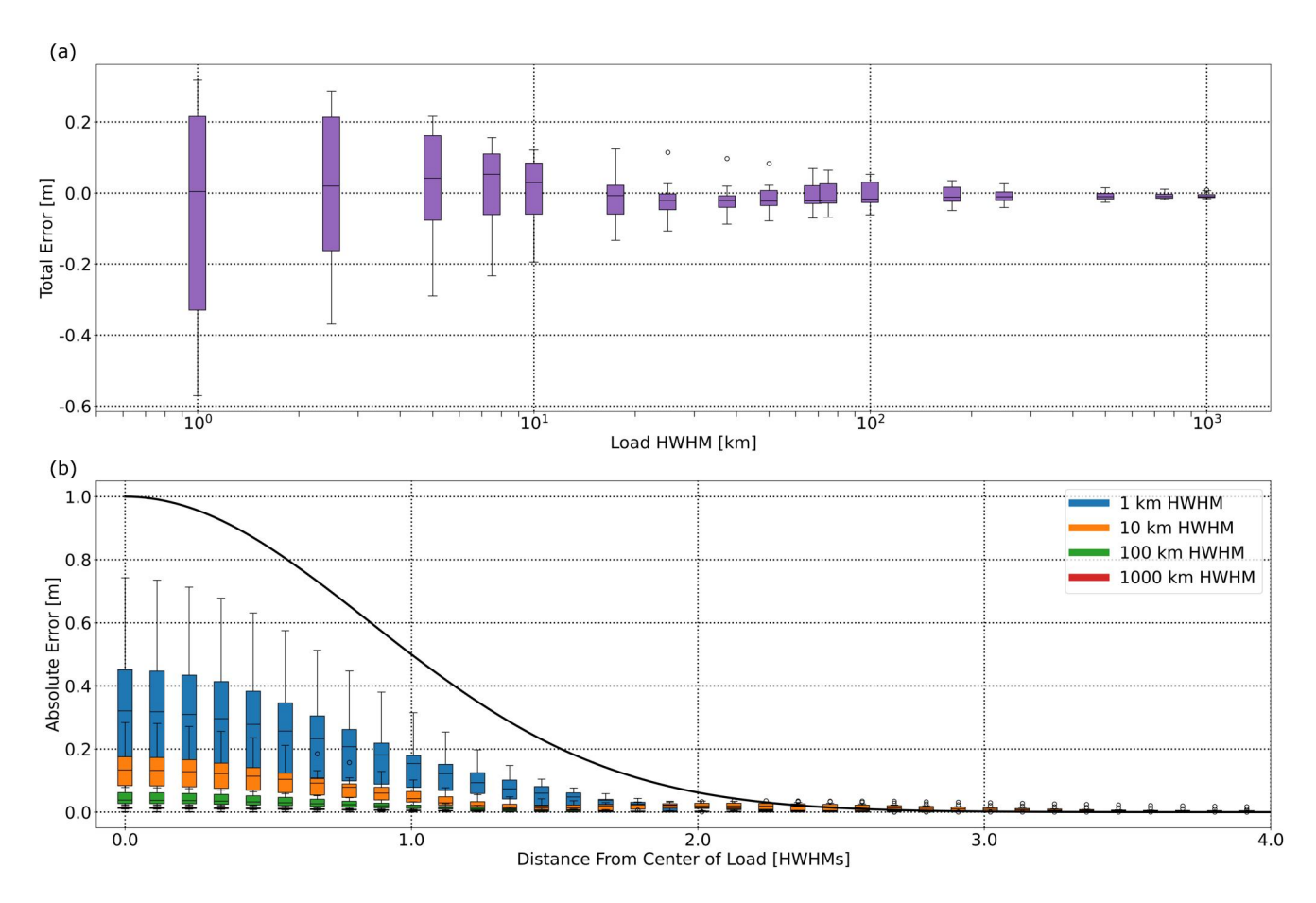


**Figure 4.** Box and whisker plots with median, quartiles, and outliers are used to illustrate the distribution of (a) total error in recovered surface load between estimates of surface load derived from vertical displacements using the eight Earth models considered here and the *true* load model as a function of load HWHM size and (b) the absolute value of error as a function of distance from the center of the load models shown in Figure 3. Load HWHM along the *x*-axis of (a) is displayed on a logarithmic scale. As the load models used here only vary in size, but retain their Gaussian geometry, distances on the *x*-axis of (b) are plotted as half width lengths away from the center of the load model. For reference, the black line represents the profile of the input Gaussian load model used to produce synthetic displacements.

ranges, however, such as STW105 and AK135f, become increasingly large relative to the error for other models that deviate from PREM primarily in the crust and upper mantle (Figures S2–S5 in Supporting Information S1).

As expected, differences between the estimated and true load's values can be related to differences in LGFs between the SNREI Earth models used to generate the data vector, d, and the design matrix, G, of the inverse problem. For instance, the LGFs for SNA exhibit smaller absolute displacements relative to PREM within the angular-distance range of  $0.001^{\circ}$ – $0.1^{\circ}$  (due to greater rigidity at shallow depths), which would correspond to smaller surface displacements for loads distributed across a similar spatial wavelength (Figure S1 in Supporting Information S1). When inverting the synthetic displacements that reflect PREM's response to the input load, a design matrix corresponding to SNA overestimates the true load's value for km-scale loads (e.g., Figure 3a). This is the result of SNA producing smaller amplitude displacements relative to PREM when an identical load is applied to both. If the data vector, d, consists of displacements derived from a "soft" Earth model (in this case, PREM) relative to a "hard" Earth model described by the design matrix, G, there will be a systematic overestimation of the load's value (i.e., water height in each grid cell) relative to the true load. Similar relationships are found for Earth models with LGFs that exhibit displacement amplitudes greater than those of PREM, such as 1066A—the estimated load's value will be systematically underestimated relative to the true load.

In addition to increased sensitivity to Earth structure for relatively small surface loads, we find sensitivities generally follow the geometry of the Gaussian load model used to produce synthetic displacements, where the largest errors in estimated surface load are located near the center (and peak) of the load model (Figure 4b). For example, we find that error decreases by a factor of two within one half width length of the center of the load.

SWARR ET AL. 8 of 21

Similarly, for distances greater than two half width lengths, errors tend to be less than 5% of the load model's true value, irrespective of the load model's spatial wavelength. Such findings are consistent with previous studies that have found differences in predictions of surface loading between Earth models are maximized in areas where the amplitude of surface loading is relatively large or at short observer-to-load distances (e.g., Argus et al., 2017; Ito & Simons, 2011; Martens, Simons, et al., 2016). Our findings highlight the potential impact of an incorrect assumption about the Earth's interior structure on GNSS-inferred estimates of TWS made across broad regions. For instance, when estimating variations in storage within the region surrounding the Sierra Nevada of California (e.g., Enzminger et al., 2018), sensitivities to Earth structure can yield errors in estimated TWS concentrated within the mountains, where surface loading is particularly large as a result of the seasonal accumulation of rain and snow, with errors quickly decaying in adjacent regions where the amplitude of surface loading is small relative to the nearby mountains.

While this appears to be generally true, we find for particular Earth model-load model combinations, the largest errors in recovered surface load can be shifted away from the center of the load (Figures S6–S8 in Supporting Information S1). We postulate that these increased errors away from the center of the load model result from differences in the elastic and density structure of a chosen Earth model with that of PREM over a specific depth range. For example, an inversion assuming the structure of CR exhibits peak error in recovered surface load for a 25 km HWHM load at a distance of 30 km from the center of the load model. When comparing the elastic and density structure of PREM and CR, we find there to be a ~2.7% reduction in the elastic and density parameters of CR relative to PREM between depths of 24–40 km. Similarly, we find that comparison of the LGFs for the Earth models considered here reveals differences that can peak at angular distances away from the center of the load (Figure S1 in Supporting Information S1).

To further assess the sensitivity of TWS estimates to assumed Earth structure, we reproduced the analysis above while incorporating both vertical and horizontal components of surface displacement in the design matrix, G, and data vector, d, of Equation 1. Overall, we find that the use of horizontal displacements in the synthetic tests presented here modulates errors in recovered water load by a few percent compared to those derived from vertical displacements alone (Figures S9–S13 in Supporting Information S1). Errors for loads with HWHM lengths less than 10 km are found to be modified by up to  $\sim$ 5% when incorporating horizontal displacements. For loads with HWHM lengths greater than 10 km, errors are only modified by up to 2%. Although incorporating horizontal displacements here only slightly modifies errors in recovered water load we believe future work could improve our understanding of sensitivities to Earth structure when using horizontal displacements by considering geodetic networks that are irregularly spaced, in contrast to the evenly spaced grid of synthetic stations used here (Figure 2), and more diverse surface load geometries.

The results here display the impact of an incorrect assumption about the Earth's interior structure when using geodetic observations of surface loading across spatial scales relevant to the management of freshwater resources. For example, an incorrect assumption about the Earth's local crustal properties may yield errors nearly as large as 0.8 m when considering 1 m of freshwater spread uniformly over a region of a few square kilometers. Hydrogeodesists and water managers must be aware of the biases that can be introduced through assumptions about Earth structure in the modeling process, since uncertainties in estimated TWS can be significant, especially at small spatial scales.

## 3. Western U.S. Case Study

Building upon the results of the previous section, we consider a case study for the western U.S. that explores the impact of Earth structure on inversions for TWS that use real geodetic data. When working with real data, we do not know the true structure of the Earth, yet we must still select an Earth model to construct the design matrix of the inverse problem. Furthermore, hydrologic loads can exhibit highly heterogeneous spatial patterns across a range of spatial and temporal scales (Skøien et al., 2003). Additionally, the distribution of GNSS stations used to estimate variations in TWS are non-uniformly distributed, which can affect the ability to resolve variations in TWS occurring at relatively fine spatial scales.

To further assess the effect of assumed Earth structure on TWS estimates derived from observations of surface loading and quantify the associated uncertainty using real data, we consider seasonal variations in TWS in the western U.S. between 1 January 2006 and 30 September 2022. We selected the western U.S. as an illustrative and relevant example as (a) the region contains a dense network of GNSS stations allowing for estimates of TWS to be

SWARR ET AL. 9 of 21

made at a relatively fine spatial scale (approx. 25 km); (b) many stations in the region have long and continuous periods of record, allowing for variations in TWS associated with prolonged periods of drought and precipitation to be made; and (c) the application of space geodetic observations to estimate changes in TWS within the region has been a topic of increasing interest over the past decade in light of several cycles of major drought and recovery (e.g., Argus et al., 2014, 2022; Borsa et al., 2014; Carlson et al., 2022).

### 3.1. Isolating Seasonal Hydrologic Loading

For this case study, we consider vertical displacements observed within the western U.S. (defined as  $31.75^{\circ}$  N  $-50.25^{\circ}$ N,  $124.75^{\circ}$ W  $-103.25^{\circ}$ W) associated with seasonal fluctuations of storage within hydrologic reservoirs. We initially obtain 2,961 daily vertical GNSS station time series estimated by the Nevada Geodetic Laboratory (NGL) in the IGS14 reference frame (Blewitt et al., 2018; Kreemer et al., 2018). We neglect the use of horizontal displacements here as the horizontal components of many GNSS stations in the western U.S. are strongly influenced by non-hydrologic sources of deformation such as tectonic interseismic, postseismic, and slow slip transient motions.

To isolate the effect of seasonal changes in TWS on station positions, we carried out the following postprocessing steps: (a) identify and discard stations with less than 5 years of data during our period of study (January 2006–September 2022); (b) remove predicted vertical displacement associated with nontidal atmospheric and nontidal oceanic loading using daily averaged estimates from the German Research Center for Geosciences Postdam (GFZ) (Dill & Dobslaw, 2013); (c) estimate and remove vertical displacement associated with glacial isostatic adjustment (GIA) using estimates from ICE-6GD (VM5a) (Peltier et al., 2018); (d) remove segments of data shorter than 60 days and separated by other data by at least 60 days, as these isolated segments may reflect station-specific equipment malfunctions; (e) remove time series offsets larger than 8 mm associated with known earthquakes and equipment changes using a catalog of known events and offset amplitudes provides by the GAGE facility (Herring et al., 2016); (f) for coseismic offsets larger than 40 mm, fit and remove a logarithmic decay model to characterize post seismic relaxation (Kreemer et al., 2006); (g) remove outliers using a median absolution deviation (MAD) filter with a running median window of 30 days and a median absolute deviation threshold factor of 10; (h) fit and remove the linear trend from each time series to remove secular signals such as uplift associated with periods of drought from the station positions; (i) convert daily position estimates into mean monthly estimates; (j) remove elastic deformation produced by variations in TWS occurring outside of the western U.S. by forward modeling displacements inferred from the Jet Propulsion Laboratory's monthly GRACE mascon solution (version RL06.1M) (Landerer et al., 2020; Watkins et al., 2015; Wiese et al., 2016) using the Earth model PREM; and (k) estimate and remove each year's mean vertical position to remove displacements associated with interannual variations in TWS (i.e., interannual drought and wet periods). We follow the procedure described in Argus et al. (2022) for interpolating GRACE estimates of TWS to periods in which GRACE or GRACE-FO estimates are unavailable. We include visualizations of the post-processing steps described here for select GNSS stations in Supporting Information S1 (Figures S14 and S15).

Following these steps, we identify stations that exhibit peak vertical uplift during the winter months to be exhibiting poroelastic behavior associated with the filling of local aquifers. We identify and remove 134 stations exhibiting poroelastic behavior. Additionally, we identify and remove 30 stations dominated by volcanic deformation primarily near the boundaries of the Long Valley Caldera and the Yellowstone hotspot. Finally, we remove 16 stations predominately located near the epicenters of the Baja and Ridgecrest earthquakes that have been strongly biased by postseismic transients. Following these steps and subsequent removals, we are left with seasonal changes in vertical position for 1,685 stations within the study region. As the time series for some stations are not continuous throughout the duration of this study, each time step in the inversion contains a varied number of observations in the data vector. The final list of stations chosen to be used in this study can be found in Supporting Information S1 (Data Set S1).

### 3.2. Estimating Seasonal Variations in TWS From Observed Vertical Displacement

We performed an inversion of the observed monthly averaged vertical displacements to estimate monthly changes in seasonal TWS in the western U.S. between January 2006 and September 2022 on a regular model grid with a resolution of  $1/4^{\circ}$ . Following a similar approach as that described in Section 2., we minimize the damped least squares problem where  $G_i$  represents the design matrix associated with assumed SNREI Earth model i. All

SWARR ET AL. 10 of 21

estimates of TWS reported here are considered anomalies relative to the January 2006–September 2022 temporal mean.

Due to the uneven distribution of GNSS stations in the region, particularly along the eastern portion of our study area, we find there can be large mass anomalies we deem nonphysical (Figure S16 in Supporting Information S1). We hypothesize that these features are the result of a lack of observational constraints in these regions, as well as geophysical signals that were not removed or improperly removed during the post-processing steps described in Section 3.1. To prevent such features from biasing our estimates of TWS, we incorporate additional constraints on the size of the model, by applying zeroth-order Tikhonov regularization (Aster et al., 2019). Thus, to estimate changes in TWS in the western U.S., we augment Equation 1 as follows:

$$\|(G_i m - d)\|_2^2 + \alpha^2 \|(Lm)\|_2^2 + \beta^2 \|(m)\|_2^2$$
(2)

where  $\beta$  is the added regularization parameter that controls the relative amplitude of the model parameters. Like many inverse problems, the problem is ill-posed and under-determined, thus the problem is non-unique. The regularization parameters  $\alpha$  and  $\beta$  act to limit the number of solutions, m, that can adequately fit the data vector, d. We use the L-curve criterion (Hansen, 1992), to determine optimal values of  $\alpha$  and  $\beta$  that minimize the residual between the best-fit model and data vector while keeping solutions smooth and parameter amplitudes relatively small. Through L-curve analysis, we find the optimal values of  $\alpha$  and  $\beta$  to be 2.5 and 1.0 respectively. As the added regularization parameter effectively reduces anomalous mass changes along the edges of the model domain, we neglect extending the boundaries of the model domain to account for edge effects as we did in Section 2.

#### 3.3. Sensitivity of Estimated Seasonal Hydrologic Loading to SNREI Earth Structure

We now compare monthly TWS estimates derived from the suite of Earth models introduced in Section 2.1. For this case study, we omit two Earth models (SNA and CR) that reflect continental shield and cratonic structure respectively as they would improperly describe the material properties and structural features of the western U.S. Additionally, we note that the LITHO1.0 model constructed to reflect the average crust and upper mantle structure of the SST River Basin contains thick sedimentary units in the uppermost crust associated with confined aquifer units that are found within the river basin. As storage-driven changes in pressure within the confined aquifer units yield a poroelastic response, many GNSS stations within the central portion of the SST were discarded in our post-processing steps. Thus the LITHO1.0 model for the SST may slightly misrepresent the crustal structure beneath many GNSS stations within our study region. However, we retain the model in our analysis to improve our understanding of how local crust and upper mantle structure, which can differ significantly from globally averaged estimates of Earth structure, affect estimates of TWS.

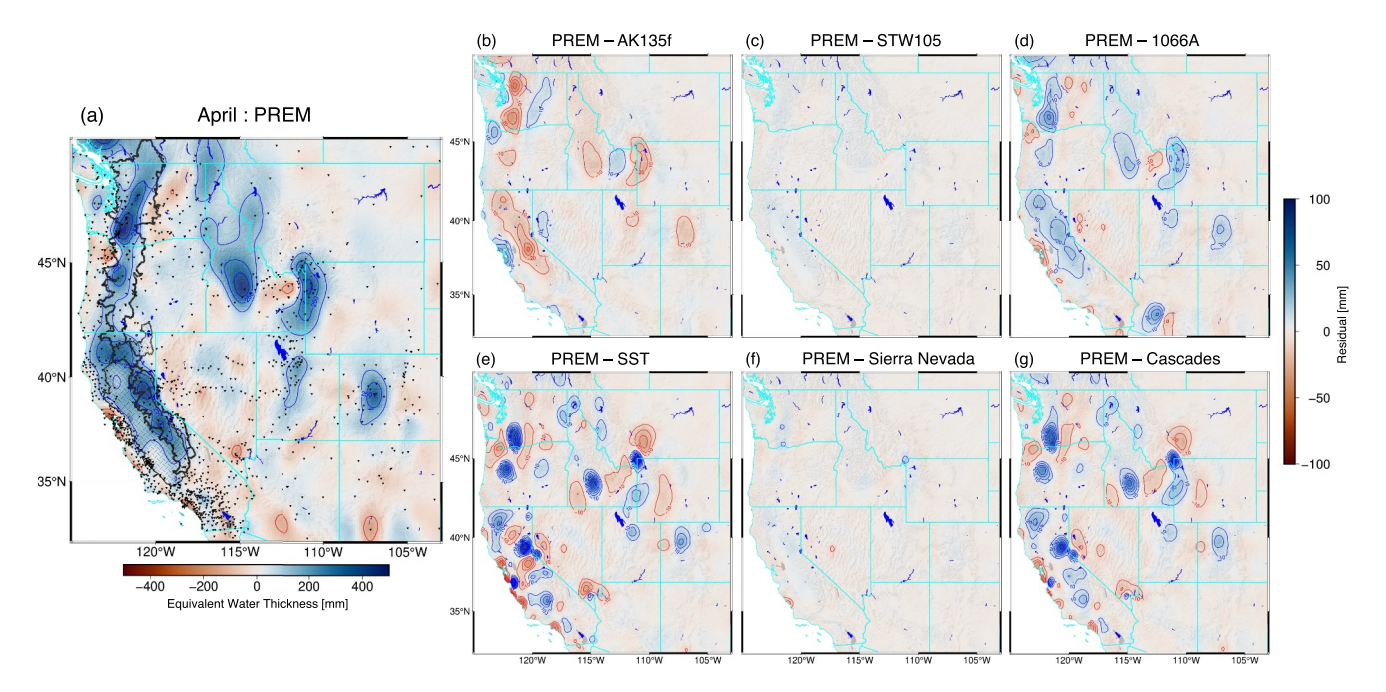
To develop a general understanding of the sensitivity of seasonal TWS estimates in the western U.S., for each Earth model used here we compute monthly stacked estimates of TWS throughout the study period. It should be noted that while monthly stacked estimates of storage allow us to consider the sensitivity of TWS estimates to Earth structure during a "typical" seasonal fluctuation in storage within the region, there can be considerable interannual variation in seasonal amplitude of TWS associated with years of higher/lower than average winter precipitation (e.g., Enzminger et al., 2019), which may result in increased/decreased sensitivity to Earth structure owing to variations in seasonal amplitude (Figure 7a).

Figure 5 depicts the monthly stacked estimate of storage for the month of April assuming PREM and the direct difference between estimates derived from the other Earth models considered here. For the month of April, mountainous regions of the western U.S., such as the Sierra Nevada and Cascade Range are estimated to have high amplitude seasonal changes in storage within surface and subsurface reservoirs as large as 300 mm of equivalent water thickness relative to the mean annual storage. Adjacent regions are estimated to experience declines in storage during the month of April, such as the Willamette Valley of Oregon, or report lower amplitude changes in storage, typically less than 100 mm of equivalent water thickness, for the month of April.

As peaks in storage are estimated to occur primarily within mountainous regions during the month of April, we find the largest discrepancies between estimates derived from different Earth models within these regions (Figures 5b–5g). For example, differences in estimated storage derived from PREM and other Earth models that represent globally averaged estimates of Earth structure, such as AK135f and 1066A, can be as large as 40 mm in

SWARR ET AL. 11 of 21

21699356, 2024, 3, Downloaded from https://agupubs.onlinelibrary.wiley.com/doi/10.1029/2023JB027938 by University Of Montana Mansfield Library-Scrials, Wiley Online Library on [11032024]. See the Terms



**Figure 5.** (a) Multi-year monthly stacked estimate of seasonal change in storage for the month of April. Sharp black lines define the boundaries of the HUC-8 watersheds within the Sierra Nevada and Cascade Range respectively. The thin black lines represent the boundary of the SST River Basin of California with a gray hatched region representing the area within the river basin. Black inverted triangles represent GNSS stations within the western U.S. used to constrain variations in seasonal TWS. Contours represent 125 mm intervals of equivalent water thickness. Direct differences between pairs of TWS estimates for the month of April using select Earth models: (b) PREM and AK135f, (c) PREM and STW105, (d) PREM and 1066A, (e) PREM and LITHO1.0 model for the SST River Basin, (f) PREM and LITHO1.0 model for the Sierra Nevada, and (g) PREM and LITHO1.0 model for the Cascade Range. The color bar at right denotes the magnitude (or size) of the residuals between TWS estimates. Contours represent 10 mm residual intervals of equivalent water thickness.

equivalent water thickness and extend across broad regions of the western U.S., typically spanning the entire length of mountain ranges, such as the Sierra Nevada (e.g., Figure 5b). Conversely, regions estimated to have relatively small amplitude changes in seasonal storage exhibit differences that are typically less than 10 mm in amplitude. Discrepancies between estimates derived from PREM and STW105 tend to be on the order of 5 mm or less extending across broad regions of the western U.S. When considering differences between estimates of TWS derived from PREM and LITHO1.0 models constructed to reflect the local Earth structure of specific regions within the western U.S., we find differences as large as 90 mm of equivalent water thickness, but such discrepancies are confined to relatively small areas within the study region, such as the area surrounding Lake Tahoe of California and Nevada (e.g., Figure 5e).

Figure 6 depicts the monthly stacked estimate of seasonal storage for the month of October. In contrast to estimates for the month of April when storage is typically at its annual maximum in the western U.S., October is often characterized as the time of the year in which storage is at its annual minimum, as precipitation in the form of rain and snow is negligible in a majority of the western U.S. and water has been lost to runoff and evapotranspiration over the warm summer months. As such, it is expected that our estimates of seasonal TWS in the western U.S. for the month of October are predominately negative and nearly equal in amplitude to estimates made for the month of April. For example, we find most mountainous areas to exhibit average storage deficits equal to 250 mm of equivalent water thickness. Similar to the month of April, when comparing estimates made assuming different models to represent the structure of the Earth, the largest discrepancies are found in regions experiencing the highest amplitude changes in seasonal storage. Discrepancies in estimated TWS between PREM and other globally averaged estimates of Earth structure yield differences as large as 30 mm spanning broad regions that align with major mountain provinces of the western U.S. Estimates of TWS assuming the local LITHO1.0 models can differ from estimates made assuming PREM within relatively small areas by over 80 mm of equivalent water thickness. Estimates of seasonal TWS and direct differences between the Earth models considered here for other months are included in Supporting Information S1 (Figures S17–S26).

As water storage dynamics in the western U.S. have been found to be closely tied to the annual accumulation and melting of snowpack deposited in mountains during winter months (e.g., Brown et al., 2008), we find it reasonable

SWARR ET AL. 12 of 21

doi/10.1029/2023JB027938 by University Of Montana Mansfield Library

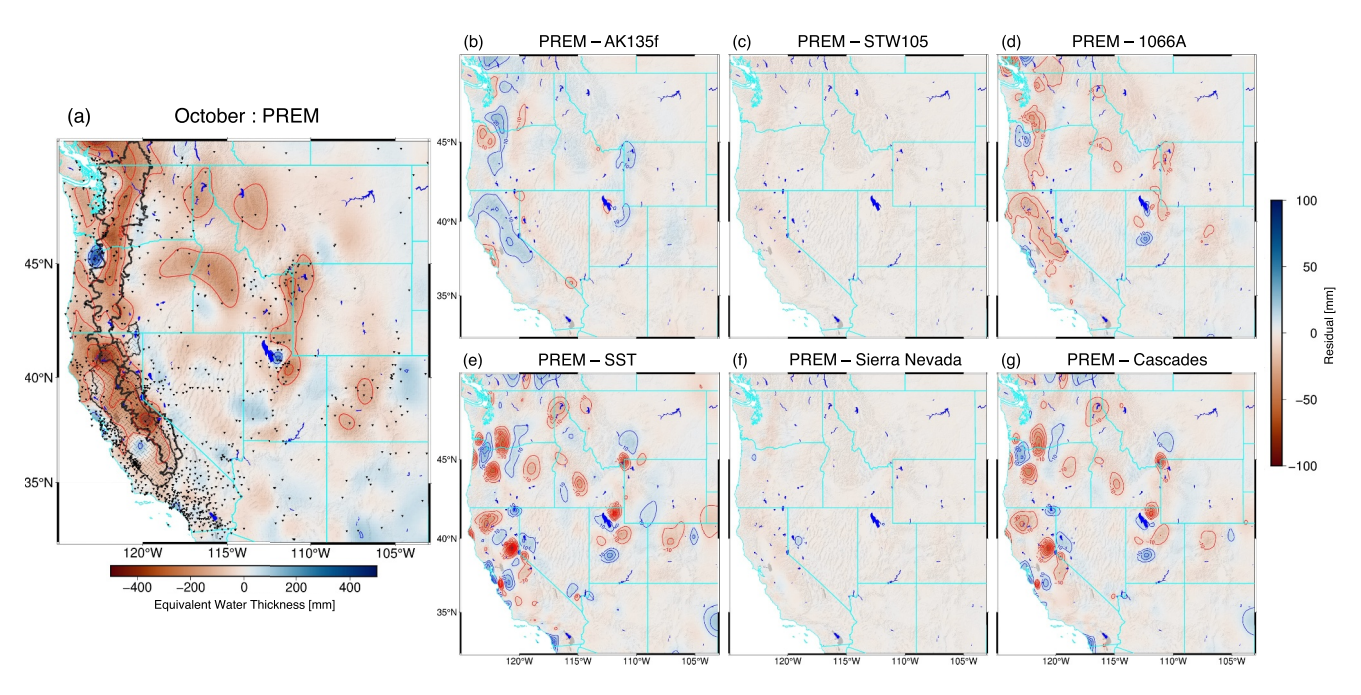


Figure 6. (a) Same as Figure 5, but for the month of October.

that estimates of seasonal TWS would exhibit the largest sensitivities to Earth structure in mountainous areas where the seasonal accumulation of precipitation is relatively large. In addition, we find the discrepancies displayed in Figures 5 and 6 between Earth models to reflect differences in the material properties of each Earth model being used here. For example, the local LITHO1.0 models may contain thick sedimentary units in the uppermost crust of the Earth, yielding LGFs with greater displacement in the near-field compared to PREM (Figure S1 in Supporting Information S1). As a result, estimates of TWS derived from the LITHO1.0 models tend to differ from estimates made with PREM by a relatively large amount over small distances (Figures 5 and 6). These differences may reflect GNSS stations observing localized hydrologic loading, such as changes in storage within a nearby lake or artificial reservoir. However, we note that the estimates derived from the LITHO1.0 model for the Sierra Nevada, which lacks sedimentary units in its uppermost crust, differ from estimates assuming the structure of PREM by less than 10 mm of equivalent water thickness. In contrast, the material properties of the other Earth models being considered tend to differ from PREM over much broader depth ranges, resulting in larger sensitivities to loading occurring within the mid-field. Discrepancies spread across many layers yield relatively smaller amplitude discrepancies in estimates of TWS that span much broader regions of the western U.S.

We now consider the effect of differences in assumed Earth structure on estimates of seasonal TWS within specific mountain and agricultural provinces vital for the effective management of freshwater resources within the western U.S. Figure 7 displays estimates of seasonal TWS for the SST River Basin, Sierra Nevada of California and the Cascade Range of Washington, Oregon, and northern California derived from the suite of Earth models considered here. Boundaries for each province are depicted as black or hatched regions in Figures 5 and 6 and are defined by the boundaries of watersheds within each region. We find that estimates of storage can differ by up to 12.4%, 13.6%, and 9.8% of the annual oscillation of storage within each of these regions respectively, and are maximized in spring and fall months when storage within hydrologic reservoirs is assumed to be at its annual maximum/minimum.

Of the Earth models considered here, we find AK135f to yield the most discrepant estimates of TWS within the western U.S. When discarded from our analysis, we find estimates of TWS within the SST, Sierra Nevada, and Cascades to vary by 6.7%, 7.2%, and 5.4% respectively. Inspection of the LGFs of AK135f reveals relatively small displacements at angular distances between 0.001 and 1.0° compared to the LGFs of the other Earth models considered here (Figure S1 in Supporting Information S1). Such discrepancies between LGFs may be partly explained by AK135f containing a relatively rigid elastic structure in the upper 80 km of the Earth (Figure 1). Furthermore, such discrepancies may indicate that hydrologic surface loading estimated from the inversion of

SWARR ET AL. 13 of 21



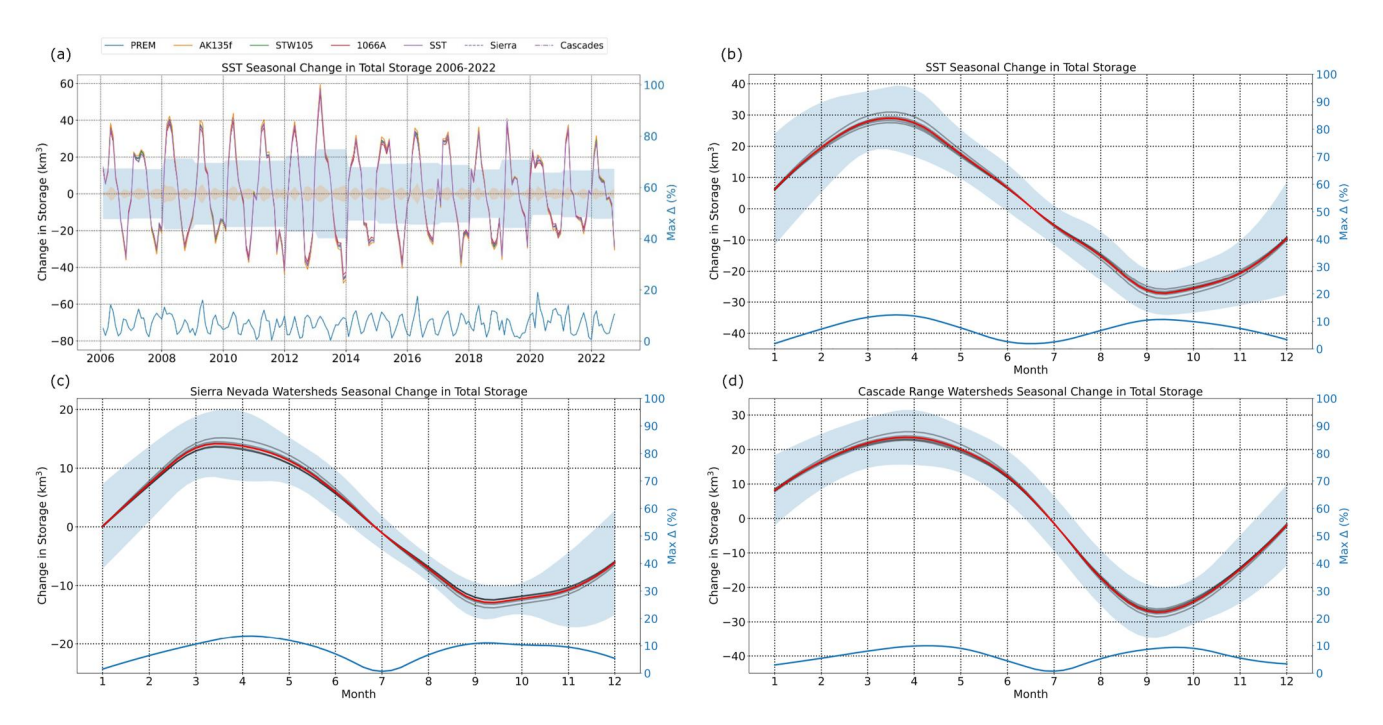


Figure 7. Estimated change in volumetric storage (km³) between January 2006 and September 2022 in the (a) SST River Basin. The yellow shaded area depicts the maximum difference in estimated storage between the Earth models used here. The solid blue line represents the maximum percentage difference between estimates of storage relative to that year's annual amplitude (blue shaded area). (b–d) Multi-year monthly stacked estimates of storage within the SST River Basin, Sierra Nevada of California, and the Cascade Range of Washington, Oregon, and northern California. The red line depicts the estimated mean seasonal fluctuation in storage within each region considering estimates derived from the seven Earth models used here (light gray lines). The light blue line depicts the maximum percentage difference between residuals derived from the set of Earth models considered here relative to the estimated mean seasonal amplitude of all models. The blue shaded area depicts the standard deviation of seasonal storage considering the full time series of monthly TWS estimates between January 2006 and September 2022.

GNSS data recorded with the western U.S. is characterized by a spatial wavelength on the order of tens of kilometers, increasing sensitivities to differences in structure between a chosen a priori Earth model and the *true* structure of the Earth over roughly equivalent depth ranges (Martens, Rivera, et al., 2016).

When estimating seasonal changes in storage within individual mountain and agricultural provinces of the western U.S., we find that estimates assuming different models for the interior structure of the Earth differ by less than 14%, and differences in estimates of storage remain small relative to reported formal uncertainties of GNSS-inferred TWS estimates within the region (e.g., Argus et al., 2017; Carlson et al., 2022). Nonetheless, water managers and policymakers should be mindful of the uncertainties associated with specific assumptions underlying the models used to convert geodetic measurements into estimates of TWS. The results presented here, however, apply specifically to the western US. Region-specific assessments should be performed when estimating uncertainties in TWS estimates for other locations and loading applications. The true error in estimated TWS associated with assumed Earth structure may be larger if the Earth models considered here differ substantially from the true structure of the region.

Additionally, the results of Section 2 as well as the comparisons of seasonal TWS between PREM and the local LITHO1.0 models point out that as the spatial scale of surface loading becomes increasingly fine, sensitivity to Earth structure can have a significant effect on estimates of TWS. As such, we find the current spatial resolution of GNSS-inferred estimates of TWS within mountain and agricultural provinces of the western U.S. (~25 km × 25 km) are subject to minor biases associated with assumed Earth structure. However, as it becomes of increasing interest to use geodetic methods to constrain storage within individual watersheds and even smaller areas, lack of knowledge of the local crust and upper mantle structure of a region may yield estimates of TWS that are significantly biased by choice of Earth model. Moreover, as GNSS networks in the western U.S. become increasingly dense, and non-hydrologic processes that deform the Earth are more accurately modeled and removed from GNSS time series, uncertainties of GNSS-inferred TWS estimates associated with Earth structure may become increasingly significant.

SWARR ET AL. 14 of 21

## 4. Predicted Global Hydrologic Loading

While the previous sections provide an awareness of the scale dependence of error in GNSS-inferred TWS estimates and the sensitivity of seasonal TWS estimates in the western U.S. to assumed Earth structure, we have only considered the effect of assumed Earth structure for surface loads that are invariant in time (Section 2.) or oscillate at an annual time scale (Section 3.). However, in many regions, hydrologic and cryospheric reservoirs have seen significant changes in storage over the past several decades associated with modern shifts in climate and an increasing reliance on groundwater to meet human needs as the global population grows (e.g., Paolo et al., 2015; Rodell et al., 2018; Seo et al., 2023; Wada et al., 2010). As such, loading and unloading of the solid Earth associated with long-term storage variations produces measurable changes in the Earth's figure and gravity field which can be used to constrain decreases in groundwater storage associated with multi-year drought (e.g., Argus et al., 2017, 2022; Liu et al., 2022), mass loss from the planet's ice sheets and glaciers (e.g., Sasgen et al., 2020; Wouters et al., 2019), and changes in global mean sea level (e.g., Jeon et al., 2018; Reager et al., 2016).

In addition to constraining variations in storage within hydrologic and cryospheric reservoirs, observations of surface displacement may be compared with predictions (typically assuming an SNREI Earth model) that characterize deformation of the Earth's surface produced by the Earth's elastic response to modern-day changes in the distribution of surface and near surface mass and the viscous response to older loading/unloading events through processes such as glacial isostatic adjustment. Through such comparisons, it is possible to acquire information about the viscosity structure of the Earth's mantle (Koulali et al., 2022; Nield et al., 2014; Velicogna & Wahr, 2002). Furthermore, by separating observations of surface displacement produced by past and present loading, area-specific sea level rise may be attributed to the individual Earth system processes producing mass redistribution as well as motion of the Earth's surface (Zanchettin et al., 2021; Ziegler et al., 2022).

As we saw in previous sections, in areas experiencing relatively large changes in storage, there is an increased sensitivity to the choice of Earth model used to model displacements produced by an applied load. As such, in regions that have experienced large-scale and systematic changes in storage within surface and near-surface reservoirs over the past several decades, such as the Greenland ice sheet, predictions of elastic displacement may be particularly sensitive to choice of Earth model. To explore this further, we next consider forward model predictions of elastic displacement produced by global variations in water storage over the past two decades.

## 4.1. Effect of Earth Structure on Predicted Surface Displacement

Using LoadDef (Martens et al., 2019), we model surface displacements produced by global hydrologic loading derived from liquid water equivalent estimates of the Jet Propulsion Laboratory's monthly GRACE mascon solution (version RL06.1M) (Landerer et al., 2020; Watkins et al., 2015; Wiese et al., 2016) over a global  $1^{\circ} \times 1^{\circ}$  grid. We model displacement of the Earth's surface over the past two decades (spanning April 2002–September 2022) to identify regions experiencing strong multi-decadal changes in storage, and to estimate the discrepancies in predictions that can be introduced by assuming different models for Earth structure. Predictions of global hydrologic loading are computed assuming commonly used Earth models: PREM, AK135f, STW105, and 1066A. All predictions reported here are considered relative to April 2002.

Figure 8 shows predictions of global vertical displacement for select months between April 2002 and September 2022. Regions that have observed considerable loss of water mass stored over the past two decades such as the Greenland ice sheet, western Antarctica, and southeastern Alaska exhibit relatively large uplift. For example, we find western portions of the Greenland ice sheet are predicted to have risen between approximately 160 and 180 mm at a mean rate of 8.3 mm/yr since April 2002 through the Earth's elastic response to pervasive loss of ice stored within the ice sheet, consistent with previous findings (e.g., Tapley et al., 2019). Conversely, regions that have observed increases in hydrologic storage relative to the start of the time series exhibit subsidence (e.g., Amazon River basin in April 2022). Predictions of horizontal displacement produced by global hydrologic loading are provided in Supporting Information S1 (Figures S27 and S28).

Figures 8b–8d show differences in vertical surface displacement between pairs of forward models using different globally averaged estimates of Earth structure. The largest discrepancies between predictions are located in polar regions where significant unloading of the Earth's surface has occurred over the past two decades due to the loss of ice mass and can be as large as 20 mm for select forward model pairs. Relatively large discrepancies between

SWARR ET AL. 15 of 21

21699356, 2024, 3, Downloaded from https://agupubs. onlinelibrary.wiley.com/doi/10.1029/2023JB027938 by University Of Montana Mansfield Library-Scriak, Wiley Online Library on [11.03.2024]. See the Terms and Conditions (https://onlinelibrary

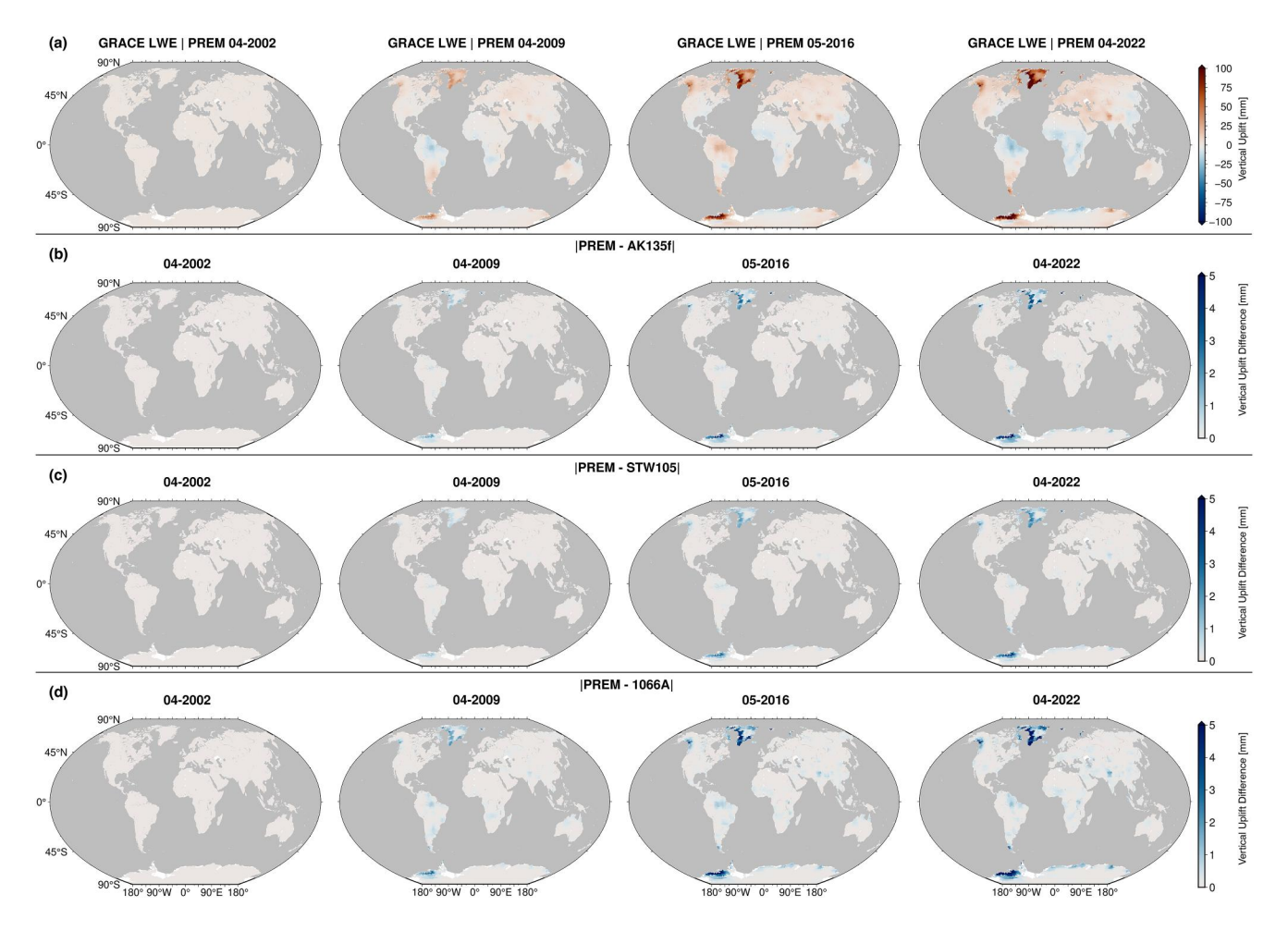


Figure 8. (a) Predicted vertical displacement for select months between April 2002 and April 2022 derived through the convolution of the LGFs of PREM with liquid water equivalent estimates of the Jet Propulsion Laboratory's monthly GRACE mascon solution (version RL06.1M) for a global 1° × 1° grid. Predicted displacements are considered relative to April 2002. The upper right color bar saturates beyond a value of 100 mm. Absolute difference in vertical surface displacement between pairs of forward models: (b) PREM and AK135f, (c) PREM and STW105, and (d) PREM and 1066A. The color bars for panels b–d depict the hydrologic-induced displacement amplitude difference between pairs of Earth models. The color bars for panels (b)–(d) saturate beyond a value of 5 mm.

forward model predictions also exist in regions that have seen increases in storage within hydrologic reservoirs over the past two decades, such as eastern Antarctica and the western Zambezi basin of Africa (Rodell et al., 2018). However, the increases in storage within these regions, and thus predicted displacement and differences between predictions derived from various Earth models, are smaller in amplitude compared to mass deficits in regions containing large ice sheets and glaciers. Differences in vertical displacement for other pairs of Earth models are provided in Supporting Information S1 (Figure S20). Predictions of horizontal displacement are similar to the vertical component in that the largest discrepancies between Earth models are located in regions experiencing large-scale changes in water mass (Figures S27 and S28 in Supporting Information S1). However, the amplitude of horizontal displacement produced by global hydrologic loading as well as discrepancies between different Earth models tend to be one or two orders of magnitude smaller than that of the vertical component.

To further investigate the effect of Earth structure on predictions of surface displacement associated with long-term changes in storage, we focus on regions that exhibit the largest discrepancies between forward model predictions at the end of the study period (Figure 8). Namely, we consider the Greenland ice sheet, western Antarctica, and southeastern Alaska, as these regions have all experienced considerable losses of mass stored within ice sheets or glaciers as a result of modern changes in global climate producing significant uplift of the Earth's surface. Time series of predicted surface displacement for individual synthetic GNSS stations (denoted by inverted triangles in Figure 9a, Figures S29a and S30a in Supporting Information S1) located within our regions of interest are displayed in Figures 9b–9d, Figures S29b–S29d, and S30b–S30d in Supporting Information S1.

SWARR ET AL. 16 of 21



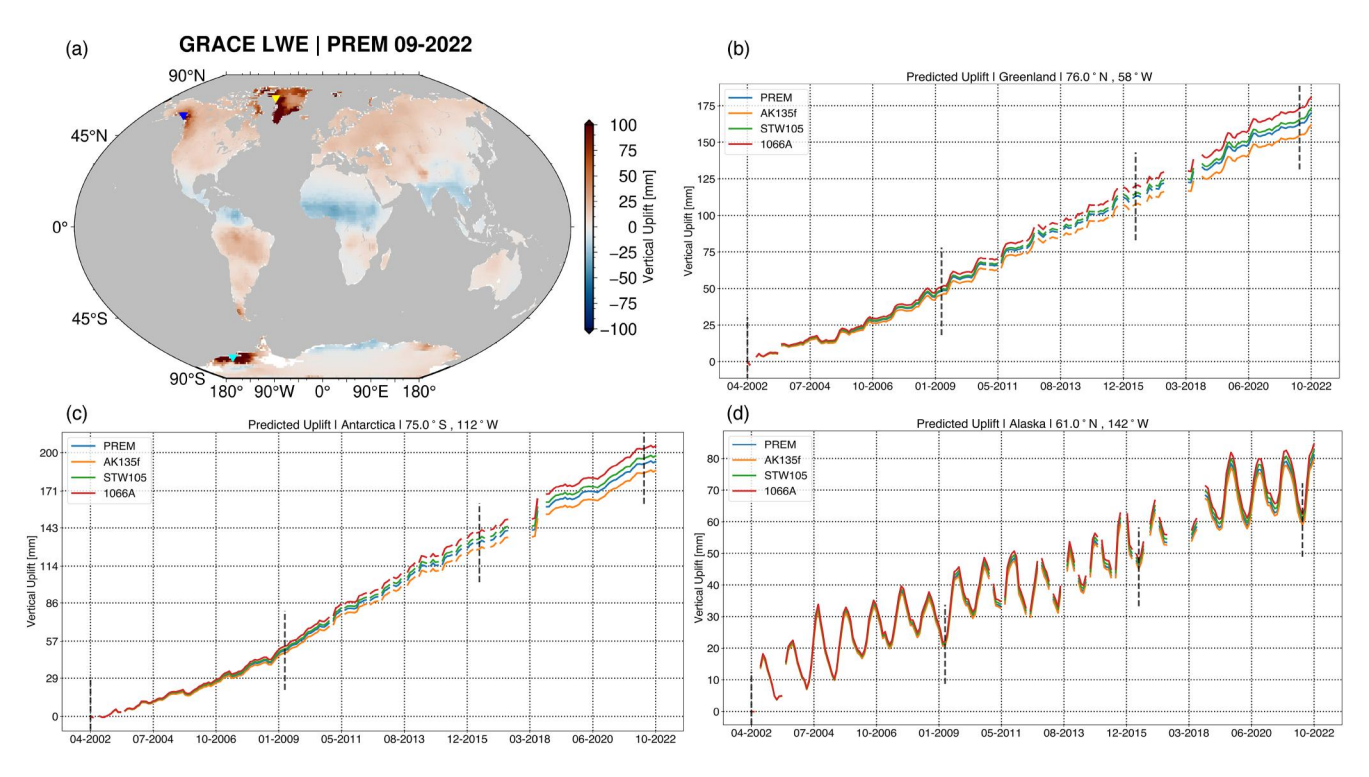


**Figure 9.** (a) Predicted vertical displacement for the month of September 2022 relative to April 2002. Inverted triangles represent sampling locations for the displacement time series depicted in panels (b–d). The color bar saturates beyond a value of 100 mm. Predictions between April 2002 and September 2022 for select Earth models at (b) 76.0°N, 58°W on the western portion of the Greenland Ice Sheet, (c) 75°S, 112°W in western Antarctica, and (d) 61.0°N, 142°W in southeastern Alaska. Gaps in predicted displacement depicted here represent data gaps in the time series of GRACE and GRACE-FO. Dashed vertical lines indicate the months in which predictions of displacement are depicted in each column of Figure 8.

Predictions of vertical displacement for the Greenland ice sheet and western Antarctica demonstrate substantial linear trends over the past two decades, attributed to continuous ice loss within these regions, with minor variability in certain years (Figures 9b and 9c). Since April 2002, these regions are predicted to have experienced between 161–181 mm and 186–205 mm of uplift, respectively. In both regions, the largest discrepancies in predictions are between AK135f and 1066A, which differ by 20 and 19 mm respectively by September 2022 and deviate from each other at a rate of nearly 1 mm per year (Figures S31a and S31b in Supporting Information S1). Conversely, the smallest discrepancies in predicted displacement are found between PREM and STW105, which differ by less than 4 mm within both regions by September 2022. Similarly, predictions in southeastern Alaska are characterized by a significant linear trend associated with mass loss from glaciers within the region, although there is also a notable seasonal oscillation in predicted displacement attributed to annual precipitation patterns (Figure 9d). Since April 2002, southeastern Alaska is predicted to have experienced between 79 and 85 mm of uplift over the past two decades. As with the other regions considered here, the largest discrepancies are between AK135f and 1066A, with a maximum difference of approximately 5 mm (Figure S31c in Supporting Information S1). The smallest discrepancies are between PREM and AK135f, with a difference of 1 mm.

We note two important findings depicted in Figure 9 and their associated implications. First, as changes in storage within hydrologic and cryospheric reservoirs are sustained over significant periods of time, acting as an increasingly large source of surface loading/unloading, discrepancies in predicted displacement between pairs of forward models become increasingly significant. For example, differences in predicted uplift of the Greenland ice sheet between forward models using PREM and AK135f increase from approximately 2.5 mm in April 2009 to over 8 mm in April 2022 (Figure S31 in Supporting Information S1). As such, when utilizing observations of surface loading to constrain changes in water storage occurring over years to decades (e.g., deglaciation, drought, groundwater depletion), the choice of Earth model becomes increasingly important as the source of surface loading becomes progressively large. As a result, storage estimates and associated interpretations may differ owing purely to the choice of Earth model. Similarly, as many regions exhibit long-term vertical deformation produced by secular trends in hydrology and glacial isostatic adjustment, prediction and subsequent removal of

SWARR ET AL. 17 of 21

elastic deformation produced by hydrologic loading may yield variable estimates of the Earth's viscous deformation response to past loading.

Second, we find that differences in predictions of long-term vertical displacement can be significantly larger than the current observational uncertainty of GNSS (~1 mm), especially in regions containing large ice sheets and glaciers. While such discrepancies pose challenges in using observations of surface displacement to constrain variations in storage within such regions, immense progress has been made over the past several decades to provide accurate estimates of mass change within the Earth's ice sheets and glaciers using satellite altimetry (e.g., Smith et al., 2020; Spada et al., 2012) and gravity field observations (e.g., Chen et al., 2006; Sasgen et al., 2019). As such, we suggest that comparison of predicted and observed surface displacement within these regions may provide an opportunity to identify and refine suitable models for regional crust and mantle structure. However, altimetry and gravity data, as well as models for mass change derived from them, also contain uncertainties that can limit the ability to use GNSS observations of surface loading to constrain Earth structure. Such information would not only provide an independent approach to constrain the interior structure of the Earth, complementing estimates derived from seismic observations but would also allow for better characterization of deformation produced by glacial isostatic adjustment within these regions.

In addition, as we used GRACE LWE estimates as the input forcing to produce displacement of the Earth's surface, we find that differences in predicted displacement between the Earth models used here can be related to the LLNs at relevant spherical harmonic degrees considering the spatial resolution of GRACE (~300 km). For GRACE, the relevant spherical harmonic degrees would be up to approximately degree 60. In general, differences in predicted displacement between Earth models for the regions highlighted here tend to differ by a similar amount as the LLNs at degree 60 (Figure S32 in Supporting Information S1). For example, we find that predictions of vertical displacement assuming the structures of AK135f, STW105, and 1066A at the synthetic GNSS station in western Greenland (76.0°N, 58°W) differ relative to PREM by approximately 4.9%, 1.7%, and 6.1%, respectively. In comparison, the LLNs describing vertical-displacement of these models at degree 60 differ relative to PREM by 5.7%, 2.6%, and 7.9%, respectively. We find these results to be consistent for the other regions highlighted as well as for the horizontal components of displacement (S29, S30). While predictions of displacement differ by approximately the same percentage as the LLNs at relevant spherical harmonic degrees, we point out that they do not differ by the exact same amount as they do for a single spherical harmonic degree (e.g., degree 60). As the input forcing used here is a global distribution of terrestrial water, there are contributions from lower degree spherical harmonics that influence the final percentage difference between predictions of surface displacement presented here.

#### 5. Conclusion

Here, we explore the sensitivity of terrestrial water storage estimates derived from observations of surface mass loading to assumed Earth structure. Through a series of synthetic loading tests, we find that as the spatial scale of surface loading becomes progressively smaller, estimates of terrestrial water storage can have errors associated with the choice of Earth model nearly as large as 80%. Thus, accurate estimates of variations in storage at relatively fine spatial scales (<10 km) require accurate knowledge of the local area's crust and upper mantle structure. Without accurate near-surface structural information, the use of geodetic observations to constrain variations in storage within relatively small hydrologic reservoirs, such as lakes and dams, may be limited. However, our results indicate that surface loads on the order of hundreds of kilometers in size are well recovered, even if the Earth model used to estimate TWS differs from the Earth's interior structure.

To determine the effect of Earth structure in a region particularly relevant in the field of hydrogeodesy, we estimated seasonal variations in GNSS-inferred terrestrial water storage within the western U.S. between January 2006 and September 2022 using multiple global and regional models for the structure of the Earth. In general, we find the largest discrepancies in estimates of seasonal TWS within mountainous regions of the western U.S., where the seasonal accumulation of rain and snow provides a large source of surface loading, enhancing differences in estimates of TWS relative to areas with small seasonal fluctuations in storage. Similarly, we find differences in estimated TWS associated with choice of Earth structure are maximized in spring and fall months when water storage within the region is at its annual maximum/minimum. Overall, we find that estimates of seasonal TWS within mountain and agricultural provinces of the western U.S. can differ by over 13% when considering different models for the Earth's interior structure.

SWARR ET AL. 18 of 21

21699356, 2024, 3, Downloaded from

Acknowledgments

We thank the editor, Shin-Chan Han, the

associate editor, an anonymous reviewer,

and Grace Carlson for their thoughtful

reviews and comments, which improved

the overall quality and readability of our

manuscript. We express gratitude to the

processing group at the Nevada Geodetic

available processed GPS data. MJS thanks

Oceanography at UC San Diego for their hospitality during the summer of 2023.

supported by NASA Earth Surface and

National Science Foundation grants EAR-

2144913. A portion of this material relied

National Science Foundation, the National

and the U.S. Geological Survey under NSF

Figures presented in this manuscript were

produced using Generic Mapping Tools

(Wessel et al., 2019) and Matplotlib

(Hunter, 2007).

Aeronautics and Space Administration.

Cooperative Agreement EAR-1724794.

Interior Grant 80NSSC19K0361 and

2218194, EAR-2021637, and EAR-

upon services provided by the GAGE

Facility, operated by the EarthScope

Consortium, with support from the

Laboratory for providing publicly

colleagues at Scripps Institution of

This material is based upon work

In addition, to consider the effect of assumed Earth structure on estimating storage and/or surface displacement associated with variations in storage within hydrologic and cryospheric reservoirs occurring over several decades, we compared predictions of global hydrologic loading over the past two decades assuming globally averaged estimates of Earth structure. Our results indicate that estimates of surface loading are particularly sensitive to choice of Earth model in regions experiencing large-scale and systematic variations in storage within reservoirs, such as the Earth's ice sheets and glaciers where predictions of uplift associated with ice loss can differ by as much as 20 mm, substantially larger than the current observational uncertainty of GNSS. Thus, given sufficiently accurate estimates of ice sheet and glacial mass loss from independent data sets, observations of the Earth's elastic response could provide new information on the elastic and density of the crust and upper mantle.

While the work presented here provides a comprehensive overview of the sensitivity of terrestrial water storage estimates derived from observations of surface displacement to assumed elastic Earth structure, we have only considered Earth models that are radially heterogeneous. In reality, the Earth's material properties are observed to vary both radially and laterally (e.g., Dannberg et al., 2017; Yuan & Romanowicz, 2018) influencing the displacement response of the Earth's surface to surface loading in regions with significant variations in three-dimensional structure, such as New Zealand (Huang et al., 2022). As the study of the solid Earth's response to climate-driven interactions between Earth systems becomes increasingly important to understand processes such as terrestrial hydrology and sea-level rise, it will be necessary to consider the impact of Earth models which deviate from the SNREI models commonly used by hydrogeodesists. Such considerations will require fully numerical simulations of surface loading which leverage approaches such as finite element or spectral element methods and will be the focus of future work.

## **Data Availability Statement**

Solution files for the synthetic tests, stations used for the inversion in Section 3, and estimates of seasonal water storage within the western U.S. for each month from January 2006 to September 2022 are publicly available at <a href="https://figshare.com/articles/dataset/Supporting\_Datasets\_for\_Sensitivity\_of\_GNSS-Derived\_Estimates\_of\_Terrestrial\_Water\_Storage\_to\_Assumed\_Earth\_Structure\_/24195357">https://grace.jpl.nasa.gov/data/get-data/jpl\_global\_mascons/</a>. GPS positions processed at the Nevada Geodetic Laboratory are available at <a href="https://geodesy.unr.edu/gps\_timeseries/tenv3/IGS14/">https://geodesy.unr.edu/gps\_timeseries/tenv3/IGS14/</a>. The LoadDef software suite can be accessed at <a href="https://github.com/hrmartens/LoadDef">https://github.com/hrmartens/LoadDef</a>.

#### References

Alterman, Z., Jarosch, H., & Pekeris, C. L. (1961). Propagation of Rayleigh waves in the Earth. *Geophysical Journal International*, 4(s0), 219–241. https://doi.org/10.1111/j.1365-246X.1961.tb06815.x

Argus, D. F., Fu, Y., & Landerer, F. W. (2014). Seasonal variation in total water storage in California inferred from GPS observations of vertical land motion. *Geophysical Research Letters*, 41(6), 1971–1980. https://doi.org/10.1002/2014GL059570

Argus, D. F., Landerer, F. W., Wiese, D. N., Martens, H. R., Fu, Y., Famiglietti, J. S., et al. (2017). Sustained water loss in California's mountain ranges during severe drought from 2012 to 2015 inferred from GPS. *Journal of Geophysical Research: Solid Earth*, 122(12). https://doi.org/10.1002/2017JB014424

Argus, D. F., Martens, H. R., Borsa, A. A., Knappe, E., Wiese, D. N., Alam, S., et al. (2022). Subsurface water flux in California's central valley and its source watershed from space geodesy. *Geophysical Research Letters*, 49(22). https://doi.org/10.1029/2022GL099583

Aster, R. C., Borchers, B., & Thurber, C. H. (2019). Parameter estimation and inverse problems. Elsevier. https://doi.org/10.1016/C2015-0-02458-3

Blewitt, G. (2003). Self-consistency in reference frames, geocenter definition, and surface loading of the solid Earth. *Journal of Geophysical Research*, 108(B2). https://doi.org/10.1029/2002JB002082

Blewitt, G., Hammond, W., & Kreemer, C. (2018). Harnessing the GPS data explosion for interdisciplinary science. *Eos*, 99. https://doi.org/10.1029/2018FO104623

Borsa, A. A., Agnew, D. C., & Cayan, D. R. (2014). Ongoing drought-induced uplift in the Western United States. *Science*, 345(6204), 1587–1590. https://doi.org/10.1126/science.1260279

Brown, T. C., Hobbins, M. T., & Ramirez, J. A. (2008). Spatial distribution of water supply in the coterminous United States <sup>1</sup>. *JAWRA Journal of the American Water Resources Association*, 44(6), 1474–1487. https://doi.org/10.1111/j.1752-1688.2008.00252.x

Carlson, G., Werth, S., & Shirzaei, M. (2022). Joint inversion of GNSS and grace for terrestrial water storage change in California. *Journal of Geophysical Research: Solid Earth*, 127(3). https://doi.org/10.1029/2021JB023135

Chen, J. L., Wilson, C. R., & Tapley, B. D. (2006). Satellite gravity measurements confirm accelerated melting of Greenland ice sheet. *Science*, 313(5795), 1958–1960. https://doi.org/10.1126/science.1129007

Chu, R., Schmandt, B., & Helmberger, D. V. (2012). Upper mantle *p* velocity structure beneath the midwestern United States derived from triplicated waveforms. *Geochemistry, Geophysics, Geosystems*, 13(2). https://doi.org/10.1029/2011GC003818

Dannberg, J., Eilon, Z., Faul, U., Gassmöller, R., Moulik, P., & Myhill, R. (2017). The importance of grain size to mantle dynamics and seis-mological observations. Geochemistry, Geophysics, Geosystems, 18(8), 3034–3061. https://doi.org/10.1002/2017GC006944

SWARR ET AL. 19 of 21

- Dill, R., & Dobslaw, H. (2013). Numerical simulations of global-scale high-resolution hydrological crustal deformations. *Journal of Geophysical Research: Solid Earth*, 118(9), 5008–5017. https://doi.org/10.1002/jgrb.50353
- Dill, R., Klemann, V., Martinec, Z., & Tesauro, M. (2015). Applying local green's functions to study the influence of the crustal structure on hydrological loading displacements. *Journal of Geodynamics*, 88, 14–22. https://doi.org/10.1016/j.jog.2015.04.005
- Dziewonski, A. M., & Anderson, D. L. (1981). Preliminary reference Earth model. *Physics of the Earth and Planetary Interiors*, 25(4), 297–356. https://doi.org/10.1016/0031-9201(81)90046-7
- Enzminger, T. L., Small, E. E., & Borsa, A. A. (2018). Accuracy of snow water equivalent estimated from GPS vertical displacements: A synthetic loading case study for Western U.S. Mountains. Water Resources Research, 54(1), 581–599. https://doi.org/10.1002/2017WR021521
- Enzminger, T. L., Small, E. E., & Borsa, A. A. (2019). Subsurface water dominates sierra Nevada seasonal hydrologic storage. Geophysical Research Letters, 46(21), 11993–12001. https://doi.org/10.1029/2019GL084589
- Farrell, W. E. (1972). Deformation of the Earth by surface loads. Reviews of Geophysics, 10(3), 761–797. https://doi.org/10.1029/RG010i003p00761
- Fu, Y., Argus, D. F., & Landerer, F. W. (2015). GPS as an independent measurement to estimate terrestrial water storage variations in Washington and Oregon. *Journal of Geophysical Research: Solid Earth*, 120(1), 552–566. https://doi.org/10.1002/2014JB011415
- Gilbert, F., & Dziewonski, A. M. (1975). An application of normal mode theory to the retrieval of structural parameters and source mechanisms from seismic spectra. *Philosophical Transactions of the Royal Society of London - Series A: Mathematical and Physical Sciences*, 278, 187–269. https://doi.org/10.1098/rsta.1975.0025
- Grand, S. P., & Helmberger, D. V. (1984). Upper mantle shear structure beneath the northwest Atlantic Ocean. *Journal of Geophysical Research*, 89(B13), 11465–11475. https://doi.org/10.1029/JB089iB13p11465
- Guo, J. Y., Li, Y. B., Huang, Y., Deng, H. T., Xu, S. Q., & Ning, J. S. (2004). Green's function of the deformation of the Earth as a result of atmospheric loading. *Geophysical Journal International*, 159(1), 53–68. https://doi.org/10.1111/j.1365-246X.2004.02410.x
- Hansen, P. C. (1992). Analysis of discrete ill-posed problems by means of the 1-curve. SIAM Review, 34(4), 561–580. https://doi.org/10.1137/1034115
- Herring, T. A., Melbourne, T. I., Murray, M. H., Floyd, M. A., Szeliga, W. M., King, R. W., et al. (2016). Plate boundary observatory and related networks: GPS data analysis methods and geodetic products. *Reviews of Geophysics*, 54(4), 759–808. https://doi.org/10.1002/2016RG000529
- Huang, P., Sulzbach, R. L., Klemann, V., Tanaka, Y., Dobslaw, H., Martinec, Z., & Thomas, M. (2022). The influence of sediments, lithosphere and upper mantle (anelastic) with lateral heterogeneity on ocean tide loading and ocean tide dynamics. *Journal of Geophysical Research: Solid Earth*, 127(11). https://doi.org/10.1029/2022JB025200
- Hunter, J. D. (2007). Matplotlib: A 2d graphics environment. Computing in Science and Engineering, 9(3), 90–95. https://doi.org/10.1109/MCSE.
- Ito, T., & Simons, M. (2011). Probing asthenospheric density, temperature, and elastic moduli below the Western United States. *Science*, 332(6032), 947–951. https://doi.org/10.1126/science.1202584
- Jeon, T., Seo, K.-W., Youm, K., Chen, J., & Wilson, C. R. (2018). Global sea level change signatures observed by grace satellite gravimetry. Scientific Reports, 8(1), 13519. https://doi.org/10.1038/s41598-018-31972-8
- Kennett, B. L. N., Engdahl, E. R., & Buland, R. (1995). Constraints on seismic velocities in the Earth from traveltimes. Geophysical Journal International, 122(1), 108–124. https://doi.org/10.1111/j.1365-246X.1995.tb03540.x
- Koulali, A., Whitehouse, P. L., Clarke, P. J., van den Broeke, M. R., Nield, G. A., King, M. A., et al. (2022). GPS-observed elastic deformation due to surface mass balance variability in the southern Antarctic peninsula. *Geophysical Research Letters*, 49(4). https://doi.org/10.1029/2021GL097109
- Kreemer, C., Blewitt, G., & Maerten, F. (2006). Co- and postseismic deformation of the 28 march 2005 Nias Mw 8.7 earthquake from continuous GPS data. *Geophysical Research Letters*, 33(7), L07307. https://doi.org/10.1029/2005GL025566
- Kreemer, C., Hammond, W. C., & Blewitt, G. (2018). A robust estimation of the 3-d intraplate deformation of the North American plate from GPS. Journal of Geophysical Research: Solid Earth, 123(5), 4388–4412. https://doi.org/10.1029/2017JB015257
- Kustowski, B., Ekström, G., & Dziewoński, A. M. (2008). Anisotropic shear-wave velocity structure of the Earth's mantle: A global model. *Journal of Geophysical Research*, 113(B6), B06306. https://doi.org/10.1029/2007JB005169
- Landerer, F. W., Flechtner, F. M., Save, H., Webb, F. H., Bandikova, T., Bertiger, W. I., et al. (2020). Extending the global mass change data record: Grace follow-on instrument and science data performance. *Geophysical Research Letters*, 47(12). https://doi.org/10.1029/
- Lettenmaier, D. P., & Famiglietti, J. S. (2006). Water from on high. Nature, 444(7119), 562-563. https://doi.org/10.1038/444562a
- Liu, P.-W., Famiglietti, J. S., Purdy, A. J., Adams, K. H., McEvoy, A. L., Reager, J. T., et al. (2022). Groundwater depletion in California's central valley accelerates during megadrought. *Nature Communications*, 13(1), 7825. https://doi.org/10.1038/s41467-022-35582-x
- Martens, H. R., Rivera, L., & Simons, M. (2019). Loaddef: A python-based toolkit to model elastic deformation caused by surface mass loading on spherically symmetric bodies. *Earth and Space Science*, 6(2), 311–323. https://doi.org/10.1029/2018EA000462
- Martens, H. R., Rivera, L., Simons, M., & Ito, T. (2016). The sensitivity of surface mass loading displacement response to perturbations in the elastic structure of the crust and mantle. *Journal of Geophysical Research: Solid Earth*, 121(5), 3911–3938. https://doi.org/10.1002/2015JB012456
- Martens, H. R., & Simons, M. (2020). A comparison of predicted and observed ocean tidal loading in Alaska. *Geophysical Journal International*, 223(1), 454–470. https://doi.org/10.1093/gji/ggaa323
- Martens, H. R., Simons, M., Owen, S., & Rivera, L. (2016). Observations of ocean tidal load response in South America from subdaily GPS positions. *Geophysical Journal International*, 205(3), 1637–1664. https://doi.org/10.1093/gji/ggw087
- Milliner, C., Materna, K., Bürgmann, R., Fu, Y., Moore, A. W., Bekaert, D., et al. (2018). Tracking the weight of hurricane Harvey's Stormwater using GPS data. Science Advances, 4(9). https://doi.org/10.1126/sciadv.aau2477
- Montagner, J.-P., & Kennett, B. L. N. (1996). How to reconcile body-wave and normal-mode reference Earth models. *Geophysical Journal International*, 125(1), 229–248. https://doi.org/10.1111/j.1365-246X.1996.tb06548.x
- Nield, G. A., Barletta, V. R., Bordoni, A., King, M. A., Whitehouse, P. L., Clarke, P. J., et al. (2014). Rapid bedrock uplift in the Antarctic Peninsula explained by viscoelastic response to recent ice unloading. *Earth and Planetary Science Letters*, 397, 32–41. https://doi.org/10.1016/j.epsl.2014.04.019
- Paolo, F. S., Fricker, H. A., & Padman, L. (2015). Volume loss from Antarctic ice shelves is accelerating. Science, 348(6232), 327–331. https://doi.org/10.1126/science.aaa0940
- Pasyanos, M. E., Masters, T. G., Laske, G., & Ma, Z. (2014). Litho1.0: An updated crust and lithospheric model of the Earth. *Journal of Geophysical Research: Solid Earth*, 119(3), 2153–2173. https://doi.org/10.1002/2013JB010626

SWARR ET AL. 20 of 21



## Journal of Geophysical Research: Solid Earth

- 10.1029/2023JB027938
- Peltier, W. R., Argus, D. F., & Drummond, R. (2018). Comment on "an assessment of the ICE-6G\_C (VM5a) glacial isostatic adjustment model" by Purcell et al. *Journal of Geophysical Research: Solid Earth*, 123(2), 2019–2028. https://doi.org/10.1002/2016JB013844
- Reager, J. T., Gardner, A. S., Famiglietti, J. S., Wiese, D. N., Eicker, A., & Lo, M.-H. (2016). A decade of sea level rise slowed by climate-driven hydrology. *Science*, 351(6274), 699–703. https://doi.org/10.1126/science.aad8386
- Rodell, M., Famiglietti, J. S., Wiese, D. N., Reager, J. T., Beaudoing, H. K., Landerer, F. W., & Lo, M.-H. (2018). Emerging trends in global freshwater availability. *Nature*, 557(7707), 651–659. https://doi.org/10.1038/s41586-018-0123-1
- Sasgen, I., Konrad, H., Helm, V., & Grosfeld, K. (2019). High-resolution mass trends of the Antarctic ice sheet through a spectral combination of satellite gravimetry and radar altimetry observations. Remote Sensing, 11(2), 144. https://doi.org/10.3390/rs11020144
- Sasgen, I., Wouters, B., Gardner, A. S., King, M. D., Tedesco, M., Landerer, F. W., et al. (2020). Return to rapid ice loss in Greenland and record loss in 2019 detected by the grace-fo satellites. *Communications Earth & Environment*, 1, 8. https://doi.org/10.1038/s43247-020-0010-1
- Seo, K., Ryu, D., Eom, J., Jeon, T., Kim, J., Youm, K., et al. (2023). Drift of Earth's pole confirms groundwater depletion as a significant contributor to global sea level rise 1993–2010. *Geophysical Research Letters*, 50(12). https://doi.org/10.1029/2023GL103509
- Skøien, J. O., Blöschl, G., & Western, A. W. (2003). Characteristic space scales and timescales in hydrology. Water Resources Research, 39(10). https://doi.org/10.1029/2002WR001736
- Smith, B., Fricker, H. A., Gardner, A. S., Medley, B., Nilsson, J., Paolo, F. S., et al. (2020). Pervasive ice sheet mass loss reflects competing ocean and atmosphere processes. *Science*, 368(6496), 1239–1242. https://doi.org/10.1126/science.aaz5845
- Spada, G., Ruggieri, G., Sørensen, L. S., Nielsen, K., Melini, D., & Colleoni, F. (2012). Greenland uplift and regional sea level changes from ICESAT observations and GIA modelling. *Geophysical Journal International*, 189(3), 1457–1474. https://doi.org/10.1111/j.1365-246X.2012.
- Tapley, B. D., Watkins, M. M., Flechtner, F., Reigber, C., Bettadpur, S., Rodell, M., et al. (2019). Contributions of grace to understanding climate change. *Nature Climate Change*, 9(5), 358–369. https://doi.org/10.1038/s41558-019-0456-2
- Velicogna, I., & Wahr, J. (2002). Postglacial rebound and Earth's viscosity structure from grace. *Journal of Geophysical Research*, 107(B12), ETG17-1–ETG17-12. https://doi.org/10.1029/2001JB001735
- Wada, Y., van Beek, L. P. H., van Kempen, C. M., Reckman, J. W. T. M., Vasak, S., & Bierkens, M. F. P. (2010). Global depletion of groundwater resources. Geophysical Research Letters, 37(20). https://doi.org/10.1029/2010GL044571
- Wahr, J., Swenson, S., Zlotnicki, V., & Velicogna, I. (2004). Time-variable gravity from grace: First results. *Geophysical Research Letters*,
- 31(11). https://doi.org/10.1029/2004GL019779
  Wang, H., Xiang, L., Wu, P., Jia, L., Jiang, L., Shen, Q., & Steffen, H. (2015). Influences of crustal thickening in the Tibetan plateau on loading modeling and inversion associated with water storage variation. Geodesy and Geodynamics, 6(3), 161–172. https://doi.org/10.1016/j.geog.
- watkins, M. M., Wiese, D. N., Yuan, D., Boening, C., & Landerer, F. W. (2015). Improved methods for observing Earth's time variable mass
- distribution with GRACE using spherical cap mascons. *Journal of Geophysical Research: Solid Earth*, 120(4), 2648–2671. https://doi.org/10.1002/2014JB011547
- Wessel, P., Luis, J. F., Uieda, L., Scharroo, R., Wobbe, F., Smith, W. H. F., & Tian, D. (2019). The generic mapping tools version 6. *Geochemistry*, *Geophysics, Geosystems*, 20(11), 5556–5564. https://doi.org/10.1029/2019GC008515
- White, A. M., Gardner, W. P., Borsa, A. A., Argus, D. F., & Martens, H. R. (2022). A review of GNSS/GPS in hydrogeodesy: Hydrologic loading applications and their implications for water resource research. Water Resources Research, 58(7). https://doi.org/10.1029/2022WR032078
- Wiese, D. N., Landerer, F. W., & Watkins, M. M. (2016). Quantifying and reducing leakage errors in the JPL RL05M GRACE mascon solution. Water Resources Research, 52(9), 7490–7502. https://doi.org/10.1002/2016WR019344
- Wouters, B., Gardner, A. S., & Moholdt, G. (2019). Global glacier mass loss during the grace satellite mission (2002–2016). Frontiers in Earth Science, 7. https://doi.org/10.3389/feart.2019.00096
- Yuan, H. & Romanowicz, B. (2018). In Lithospheric discontinuities. Wiley. https://doi.org/10.1002/9781119249740
- Zanchettin, D., Bruni, S., Raicich, F., Lionello, P., Adloff, F., Androsov, A., et al. (2021). Sea-level rise in Venice: Historic and future trends (review article). Natural Hazards and Earth System Sciences, 21(8), 2643–2678. https://doi.org/10.5194/nhess-21-2643-2021
- Ziegler, Y., Vishwakarma, B. D., Brady, A., Chuter, S., Royston, S., Westaway, R. M., & Bamber, J. L. (2022). Can GPS and grace data be used to separate past and present-day surface loading in a data-driven approach? Geophysical Journal International, 232(2), 884–901. https://doi.org/10.1093/gji/ggac365

SWARR ET AL. 21 of 21